DE-FG05-80ET-53088-675 IFSR #675

Two-Dimensional Ballooning Transformation with Applications to Toroidal Alfvén Eigenmodes
(THESIS)

X.D. ZHANG
Institute for Fusion Studies
The University of Texas at Austin
Austin, Texas 78712

October 1994

TWO-DIMENSIONAL BALLOONING TRANSFORMATION WITH APPLICATIONS TO TOROIDAL ALFVÉN EIGENMODES

APPROVED BY

DISSERTATION COMMITTEE:

Richard D. Hazeltine

Swadesh Mahajan

Philip J. Morrison

K.W. Smith

Robert E. Waltz

Dedicated to my parents.

TWO-DIMENSIONAL BALLOONING TRANSFORMATION WITH APPLICATIONS TO TOROIDAL ALFVÉN EIGENMODES

by

XIAO-DONG ZHANG, B.S.

DISSERTATION

Presented to the Faculty of the Graduate School of

The University of Texas at Austin

in Partial Fulfillment

of the Requirements

for the Degree of

DOCTOR OF PHILOSOPHY

THE UNIVERSITY OF TEXAS AT AUSTIN

December, 1994

Acknowledgments

I would like to thank Prof. Richard Hazeltine and Dr. Swadesh Mahajan for their supervision and guidance during the years of my study at The Institute for Fusion Studies. It has been a great privilege and rewarding experience to learn from and work with them. Their expertise and physical insight has always been my inspiration. In particular, I want to thank them for giving me great freedom in doing scientific research. I also want to thank Profs. Ken Gentle, Phil Morrison, and Robert Wyatt for serving on my dissertation committee.

It has been a great pleasure to collaborate with Dr. Yangzhong Zhang, who taught me many aspects of the ballooning theory and the useful apparatus of two dimensional ballooning transformation. His help, friendship and constant encouragement is gratefully acknowledged.

I am also indebted to my fellow graduate students and colleagues (present and former) at The Institute for Fusion Studies and The Fusion Research Center for their invaluable help and many discussions. Among the many are Mark Calvin, Jiayu Chen, Xiaoliang Chen, John Cobb, Jiaqi Dong, Zhen Guo, Chris Kueny, Hong Lin, Xiangning Su, Prashant Valanju, Hong Xiao, and Huanchun Ye.

I would like to acknowledge The Institute for Fusion Studies at The University of Texas at Austin for employment during the years, and the administrative staff there for their excellent work of support.

I especially want to thank Prof. T.D. Lee at Columbia University for his tremendous efforts in initiating and arranging the CUSPEA program, which brought me to The University of Texas at Austin.

Finally, I thank my parents for their love and understanding during this rather long period of time.

TWO-DIMENSIONAL BALLOONING TRANSFORMATION WITH APPLICATIONS TO TOROIDAL ALFVÉN EIGENMODES

Publication No. _____

Xiao-Dong Zhang, Ph.D.
The University of Texas at Austin, 1994

Supervisor: Richard D. Hazeltine

A general formulation for high-n (n is the toroidal mode number) modes in an axisymmetric toroidal plasma is presented, based on the two dimensional (2-D) ballooning transformation. It is shown that this formulation is more general than the conventional ballooning theory, and reduces to the conventional theory in a special case.

Toroidal Alfvén waves are studied using the 2-D ballooning formulation. A perturbation theory is systematically developed for the continuum damping of the toroidal Alfvén eigenmode (TAE). A formula, similar to the Fermi golden rule for decaying systems in quantum mechanics, is derived for the continuum damping rate of the TAE; the decay (damping) rate is expressed explicitly in terms of the coupling of the TAE to the continuum spectrum. Numerical results are obtained and compared to previous calculations.

Kinetic effects on toroidal Alfvén waves are studied. Multiple-gap coupling is included automatically by the 2-D ballooning formulation. A new branch of modes, the kinetic toroidal Alfvén eigenmodes (KTAE), emerges as a result of kinetic effects. This mode resides just above the toroidal shear Alfvén gap, and has a structure similar to the TAE. Numerical results for the kinetic damping rates for the TAE and the KTAE are obtained, and multiple-gap coupling effects are studied by comparing with the single gap theory of Mett and Mahajan [Phys. Fluids B 4 2885 (1992)].

Table of Contents

List of Tables

VITA

Xiao-Dong Zhang was born on October 27, 1964, in Xinyu, Jiangxi, The People's Republic of China, the son of Tingfu Zhang and Huaying Zhang. Upon graduating from high school, he entered Tsinghua University in Beijing, China, and received the degree of Bachelor of Science in electrical engineering in July 1986. The following fall he entered The University of Texas at Austin as a graduate student in physics. He has been employed as a research assistant in the Institute for Fusion Studies since 1989.

Permanent address: Changqing school
Xinyu, Jiangxi
The People's Republic of
China

This dissertation was typeset[1] with LaTeX by the author.

[1] LaTeX document preparation system was developed by Leslie Lamport as a special version of Donald Knuth's TeX program for computer typesetting. TeX is a trademark of the American Mathematical Society. The LaTeX macro package for The University of Texas at Austin dissertation format was written by Khe-Sing The.

List of Figures

Chapter 1

Introduction

Since its first construction in the late seventies (Refs. [1–4]), the ballooning transformation has become a standard tool for analyzing linear instabilities in toroidal plasmas. In addition to its earlier applications in theories of the ballooning instability, it has also been used in the analysis of instabilities such as the toroidal drift waves [5, 6], the ion temperature gradient driven modes (the ITG or η_i mode) [7, 8] and the toroidicity induced Alfvén eigenmodes (the TAE) [9]. In general, the ballooning representation is considered a proper tool in treating a class of high n (where n is the toroidal mode number) perturbations which have long (short) wavelength along (perpendicular to) the magnetic field ($k_{\|}/k_{\perp} \ll 1$). Perturbations with these characteristics are generally the most dangerous in a plasma since the stablizing effects of the magnetic field (magnetic line bending) are minimized. On the other hand, high n modes are often more unstable than low n modes. An important example is the high n ballooning mode, which is believed to pose a limitation on the plasma beta (the ratio of material pressure to magnetic pressure).

Because of variations of the equilibrium quantities in the poloidal direction, the analysis of linear modes in an axisymmetric toroidal plasma usually involves the solution of a two dimensional eigenvalue problem. For high n modes with long parallel and short perpendicular wavelengths (or flute-like ordering), the equation exhibits two disparate length scales: the short

scale length measureing the separation between mode rational surfaces, and the longer equilibrium scale length. A natural technique for such problems is the eikonal analysis. However, for instabilities in a toroidal plasma with magnetic shear, the eikonal representation is in contradiction with the requirement that the perturbed quantity be periodic in the poloidal angle. The conventional ballooning transform was constructed to resolve this contradiction; the original problem is replaced by a "fictitious" one obeying the same equation but defined on an infinite domain of the poloidal angle (the covering space) where the periodicity requirement can be dropped. Due to the existence of a local translational invariance (or ballooning symmetry) [3, 10, 11], an ordered expansion in $1/\sqrt{n}$ (n is the toroidal mode number) then reduces the 2-D partial differential equation to a set of two ordinary differential equations, one for the local structure around a single rational surface, and the other for the global structure combining the local modes. The physical perturbation, which is periodic, is constructed as an infinite sum of the aperiodic "covering space" solutions. In the strong ballooning case, the resulting mode is radially extended over many rational surfaces and is poloidally localized near $\theta = 0$ or π (where θ is the poloidal angle). It should be emphasized that, in addition to the obvious computational advantage, this approach also allows a better physical understanding as compared to brute force numerical solutions.

However, there are several limitations to the applicability of the conventional ballooning theory. Among others, it is required that the solution be sought at an extremum of the local mode frequency [1, 2, 12]. Therefore these type of modes are rather rare, and even if they exist, they affect only a small fraction of the plasma. For nonideal systems, it was shown that the

conventional ballooning theory encounters the problem of a complex solvability condition [10, 13]. On the other hand, recent investigations on toroidal Alfvén eigenmodes (TAE) [14, 15] showed that the TAEs have a mode structure quite different from that of the conventional ballooning picture. These modes can not be described by the conventional theory.

In this thesis, we present a new formulation of ballooning theory based on the two dimensional ballooning transformation first introduced by Zhang and Mahajan (Ref. [10]). A general description of the theory is given in Chapter 2. In order to show the basic principles of the ballooning approach, a review of the conventional ballooning theory is also given. Like the conventional theory, our formulation also relies on the approximate translational invariance (the ballooning symmetry). But instead of using an eikonal type approach, we expand the eigenfunction on a new base formed by the eigenfunctions of a translationally invariant operator. When the ballooning symmetry is only weakly violated, this procedure is more appropriate than the usual Fourier expansion in poloidal harmonics.

In Chapter 3, we demonstrate the new formalism by analytically solving the two model equations discussed in Ref. [16]. The results of Ref. [16], which were obtained in a different way, are recovered by the ballooning approach. Comparison is made to the conventional ballooning theory of Connor, Hastie and Taylor [2]. It is shown that our formulation is more general than the conventional theory, and it reduces to the conventional theory in a special case. In particular, the relationship between the conventional ballooning feature and the "other" type of ballooning shown by the resistive interchange instability is demonstrated.

In Chapters 4 and 5, we apply the theory to study the toroidal Alfvén eigenmodes (TAE). The TAE is a global mode located in the toroidicity induced shear Alfvén gap. In the ideal magnetohydrodynamic (MHD) limit with cylindrical symmetry, the shear Alfvén spectra is a continuum with $(\omega_A)_{min} < \omega < (\omega_A)_{max}$ [17, 18, 19]. The corresponding normal mode has a singularity at $\omega = \omega_A(r)$. Because of this singularity, an infinite amount of energy is needed to excite a single normal mode. All physically valid excitations must therefore consist of a superposition of normal modes. These excitations are strongly damped by phase mixing, and hence pose little danger to plasma confinement. This picture is altered qualitatively in toroidal geometry. While periodic modulations in the poloidal direction creates forbidden frequency gaps in the shear Alfvén spectrum, it also allows the existence of a discrete mode in the gap — the TAE [9, 20]. Unlike normal modes in the continuum, the TAE is not singular, and is not damped by phase mixing. In a fusion tokamak, the TAE is likely to be driven unstable by resonant interaction with fusion alpha particles. These unstable modes could in turn cause deterioration in alpha particle confinement, and hence of the self-sustained heating efficiency. Indeed, it has been shown that even low amplitude TAE's can cause severe alpha particle losses [21]. In order to give a practical estimate of the stability threshold for the TAE, all possible damping mechanisms must be considered. Stimulated by the mismatch between stability threshold predicted by earlier theories [22, 23] (in which only electron Landau damping through the curvature drifts is considered) and experimental observations [24, 25], various other damping effects on the TAE have been investigated. It has since then been found that the TAE is more effectively damped by effects such as the continuum damping [14, 15, 26], ion Landau damping [27], collisional trapped particles [28], finite

parallel electric fields (radiation damping) [29, 30], and finite Larmor radius effects [31].

Continuum damping of the TAE, caused by the resonant interaction of the TAE with the shear Alfvén continuum, is studied in Chapter 4. Within the framework of ideal magnetohydrodynamics, it has been studied recently by by Berk *et al.* [26] in the low-n (toroidal mode number) limit and by Rosenbluth *et al.* [14] and Zonca and Chen [15] in the high-n limit. It was concluded that, for typical tokamak parameters, continuum damping can be significant, even comparable to alpha particle induced growth rates. The high-n case is studied in Chapter 4. It will be shown that the ballooning approach is very convenient for the high-n TAE. The creation of gaps in the shear Alfvén continuum by poloidal modulation and the formation of the TAE's in the gaps come out quite naturally. And the continuum damping rate can be written explicitly in terms of the coupling of the TAE to the continuum spectrum. Numerical results are obtained for various plasma parameters and compared to previous calculations.

In Chapter 5, kinetic effects (finite parallel electric fields) on the TAE are studied. The importance of kinetic effects was first pointed out by Mett and Mahajan [29, 30]. It was shown that additional damping for the TAE results from the interaction of toroidicity with kinetics of Alfvén waves, and a new family of modes called the kinetic toroidal Alfvén eigenmodes (KTAE) was introduced. Their theory considered the coupling of a single pair of poloidal harmonics and thus is a single gap theory. Chapter 5 is an extension of their theory to multiple gaps for moderate to high n modes. It will be shown that multiple gap couplings are more significant for moderate to large magnetic shear. In the weak shear limit, multiple gap theory reduces to single gap

theory. It is found that multiple gap effects are less profound for the KTAE than for the TAE, consistent with the fact that the KTAE has a well defined slab limit.

Chapter 6 is a brief summary.

Chapter 2

General Description of Ballooning Theory

2.1 Review of the Conventional Ballooning Theory

In order to demonstrate the basic principles in a ballooning type approach, we give a formal development of the conventional ballooning theory in this section. We will follow the formulation of Connor, Hastie and Taylor [1, 2], because it is the most widely used.

Consider an axisymmetric toroidal system. We can introduce an orthogonal coordinate system (ψ, ζ, θ) (see, e.g. Refs. [32, 33]) where ψ is the poloidal magnetic flux which labels the magnetic surface, ζ is the azimuthal angle around the symmetric axis of the torus and θ is a poloidal angle. A field line is defined by ψ = constant, $\theta = \theta_0(\zeta)$ and $\nu \equiv (d\zeta/d\theta_0)$ measures the magnetic field line pitch, which is related to the toroidal safety factor q by $q = (2\pi)^{-1} \oint \nu d\theta$. Now for a high-$n$ (n is the toroidal mode number) perturbation with long parallel and short perpendicular wavelengths (or flute-like ordering), it is natural to use the eikonal representation [2, 32] and write the fluctuating quantities as

$$\tilde{\phi} = F(\psi, \theta) \exp\left[in\left(\zeta - \int^{\theta} \nu d\theta\right)\right], \tag{2.1}$$

where the phase varies rapidly across the magnetic field but is constant along it. Representation (2.1) would be quite appropriate if it were not for the periodicity requirement $\tilde{\phi}(\theta + 2\pi) = \tilde{\phi}(\theta)$. It can be shown that Eq. (2.1) satisfies

the periodic condition in θ only on the rational surfaces [32], and hence cannot be an acceptable representation for $\tilde{\phi}$, because $\tilde{\phi}$ must be periodic (in θ) everywhere. The ballooning representation came about as an attempt to impose requirements of periodicity on a basic eikonal representation. The essential step is to extend the poloidal angle θ into an infinite domain (the covering space), and write $\phi(\psi,\theta)$ as (where $\phi(\psi,\theta) = \exp(-in\zeta)\tilde{\phi}(\psi,\theta,\zeta)$)

$$\phi(\psi,\theta) = \sum_m e^{-im\theta} \int_{-\infty}^{\infty} e^{im\eta} \widehat{\phi}(\psi,\eta) d\eta, \tag{2.2}$$

which automatically ensures that ϕ is periodic in θ. Equation (2.2) defines the so called ballooning transformation. Note that $\widehat{\phi}$ is defined on the infinite domain $\eta \in (-\infty,\infty)$, and it need not be perodic. Since ζ is an ignorable coordinate, the equation for linear dynamics can be formally written as

$$\mathcal{L}(\psi,\partial_\psi;\theta,\partial_\theta;\Omega)\phi(\psi,\theta) = 0, \tag{2.3}$$

where Ω is the eigenvalue, and $\mathcal{L}$ is self-adjoint and periodic in θ. Direct substitution of Eq. (2.2) verifies that Eq. (2.3) is satisfied for any $\widehat{\phi}$ satisfying the same equation. Thus solution of Eq. (2.3) is replaced by the solution of the same equation in the infinite domain. Since $\widehat{\phi}$ is free of periodicity constraints, it can be written in the form

$$\widehat{\phi}(\psi,\eta) = F(\psi,\eta) \exp\left(-in \int_{\eta_0}^{\eta} \nu d\eta\right), \tag{2.4}$$

where η_0 is an undetermined arbitrary phase and F is assumed to be slowly varying. Substitution into Eq. (2.3) yields the following equation for $F(\psi,\eta)$

$$\mathcal{L}(\psi, -in\int_{\eta_0}^{\eta} \nu' d\eta + \partial_\psi; \eta, -in\nu + \partial_\eta; \Omega) F(\psi,\eta) = 0, \tag{2.5}$$

where $\nu' \equiv \partial\nu/\partial\psi$.

There are two explicit fast variables in Eq. (2.5) associated with n, one in the second argument and the other in the fourth argument. However, for flute-like modes, the fast variation in the fourth argument cancels the implicit fast variation in the first argument. And the only fast variation of $\mathcal{L}$ in Eq. (2.5) is associated with the second argument. One can then expand $\mathcal{L}$ in ascending orders of ∂_ψ. Defining

$$y = -in\int_{\eta_0}^{\eta} \nu' d\eta + \epsilon\frac{\partial}{\partial\psi}, \tag{2.6}$$

where ϵ is a formal smallness parameter, $\mathcal{L}$ can be expanded as

$$\mathcal{L} = \mathcal{L}[\epsilon = 0] + \left.\frac{\partial\mathcal{L}}{\partial y}\right|_{\epsilon=0}\frac{\partial}{\partial\psi} + \frac{1}{2}\left.\frac{\partial^2\mathcal{L}}{\partial y^2}\right|_{\epsilon=0}\frac{\partial^2}{\partial\psi^2}. \tag{2.7}$$

If we further denote the first term by a new symbol L_0

$$L_0(\psi,\eta,\Omega) \equiv \mathcal{L}[\epsilon = 0] = \mathcal{L}(\psi, -in\int_{\eta_0}^{\eta}\nu' d\eta; \eta, -in\nu + \partial/\partial\eta; \Omega), \tag{2.8}$$

then for the last two terms the following holds,

$$\frac{\partial\mathcal{L}}{\partial y} = -\frac{i}{n\nu'(\eta_0)}\frac{\partial L_0}{\partial\eta_0}$$

$$\frac{\partial^2\mathcal{L}}{\partial y^2} = -\frac{1}{n\nu'(\eta_0)}\frac{\partial}{\partial\eta_0}\left(\frac{1}{n\nu'(\eta_0)}\frac{\partial L_0}{\partial\eta_0}\right).$$

Thus the operator $\mathcal{L}$ can be cast into the form

$$\mathcal{L} = L_0 + \frac{1}{n^{1/2}}L_1\frac{\partial}{\partial x} + \frac{1}{n}L_2\frac{\partial^2}{\partial x^2}, \tag{2.9}$$

where

$$L_1 = -\frac{i}{\nu'(\eta_0)}\frac{\partial L_0}{\partial\eta_0}, \tag{2.10}$$

$$L_2 = -\frac{1}{2\nu'(\eta_0)}\frac{\partial}{\partial\eta_0}\left(\frac{1}{\nu'(\eta_0)}\frac{\partial L_0}{\partial\eta_0}\right), \tag{2.11}$$

and a more rapid length scale in the direction normal to the magnetic surfaces is introduced by $x \equiv n^{1/2}(\psi - \psi_0)$ (where ψ_0 designates some reference magnetic surface). Asymptotic solutions are then sought in ascending orders of $n^{-1/2}$, starting from the lowest order equation

$$L_0(\psi, \eta, \omega) f_0(\psi, \eta) = 0, \tag{2.12}$$

where ω is the eigenvalue. Equation (2.12) is commonly called the ballooning equation, and is clearly an ordinary differential equation in η; ψ appears only as a parameter. Assuming that

$$F = A(x) f_0(\psi, \eta) + \frac{1}{n^{1/2}} F_1(\psi, \eta) + \frac{1}{n} F_2(\psi, \eta), \tag{2.13}$$

and treating eigenvalue corrections as second order (which is justified *a posteriori*), the equations for first and second order can be respectively written as

$$L_0 F_1 + L_1 f_0 \frac{dA(x)}{dx} = 0, \tag{2.14}$$

and

$$L_0 F_2 + L_1 \frac{\partial}{\partial x} F_1 + A L_1 \frac{\partial}{\partial \psi} f_0(\psi, \eta) + L_2 \frac{\partial^2}{\partial x^2} A f_0 + n \frac{\partial L_0}{\partial \omega} A f_0 (\Omega - \omega) = 0. \tag{2.15}$$

Using the self-adjointness of the operator L_0, the integrability condition for the first order equation becomes

$$\left\langle f_0 \mid \frac{\partial L_0}{\partial \eta_0} \mid f_0 \right\rangle \equiv \int_{-\infty}^{\infty} f_0 \frac{\partial L_0}{\partial \eta_0} f_0 \, d\eta = 0. \tag{2.16}$$

Differentiating Eq. (2.12) with respect to η_0 shows that the above condition is equivalent to

$$\frac{\partial \omega}{\partial \eta_0} = 0, \tag{2.17}$$

which is satisfied at $\eta_0 = 0$ and $\eta_0 = \pi$ by the symmetry of the problem. Equation (2.14) is then easily solved for F_1 and, upon multiplying Eq. (2.15) from left by f_0 and integrating, one obtains the solvability condition for the second order equation:

$$\left[\frac{1}{\nu'^2}\left\langle f_0 \mid \frac{\partial L_0}{\partial \eta_0} \mid \frac{\partial f_0}{\partial \eta_0}\right\rangle + \frac{1}{2}\left\langle f_0 \mid \frac{1}{\nu'}\frac{\partial}{\partial \eta_0}\left(\frac{1}{\nu'}\frac{\partial L_0}{\partial \eta_0}\right) \mid f_0\right\rangle\right]\frac{d^2A(x)}{dx^2}$$

$$+\left[\left\langle f_0 \mid \frac{i}{\nu'}\frac{\partial L_0}{\partial \eta_0} \mid \frac{\partial f_0}{\partial \psi}\right\rangle - n\left\langle f_0 \mid \frac{\partial L_0}{\partial \omega} \mid f_0\right\rangle(\Omega - \omega)\right]A(x) = 0. \tag{2.18}$$

With the help of Eq. (2.17), it can be shown that

$$\left\langle f_0 \mid \frac{\partial}{\partial \eta_0}\left(\frac{1}{\nu'}\frac{\partial L_0}{\partial \eta_0}\right) \mid f_0\right\rangle + \frac{1}{\nu'}\left\langle f_0 \mid \frac{\partial L_0}{\partial \omega} \mid f_0\right\rangle\frac{\partial^2 \omega}{\partial \eta_0^2}$$

$$+\frac{2}{\nu'}\left\langle f_0 \mid \frac{\partial L_0}{\partial \eta_0} \mid \frac{\partial f_0}{\partial \eta_0}\right\rangle = 0, \tag{2.19}$$

which converts Eq. (2.18) into

$$\frac{\partial^2 \omega}{\partial \eta_0^2}\frac{d^2A(x)}{dx^2} + (\nu'(\eta_0))^2\left[2n(\Omega - \omega) - \frac{\langle f_0 \mid \frac{i}{\nu'}\frac{\partial L_0}{\partial \eta_0} \mid \frac{\partial f_0}{\partial \psi}\rangle}{\langle f_0 \mid \frac{\partial L_0}{\partial \omega} \mid f_0\rangle}\right]A(x) = 0, \tag{2.20}$$

to be solved near an extremum of $\omega(\eta_0, \psi)$. It is easily seen that the second term in the square bracket gives a small correction (of order $1/n$) to the local potential created by $\omega(x)$, and can be neglected. The final equation is

$$\frac{\partial^2 \omega}{\partial \eta_0^2}\frac{d^2A(x)}{dx^2} + (\nu'(\eta_0))^2\left[2n(\Omega - \omega(\psi_0)) - \frac{\partial^2 \omega}{\partial \psi^2}x^2\right]A(x) = 0, \tag{2.21}$$

yielding the following envelop function

$$A(x) = \exp\left[-\frac{1}{2} \mid \nu'(\eta_0) \mid \left(\frac{\partial^2\omega}{\partial\psi^2} \Big/ \frac{\partial^2\omega}{\partial\eta_0^2}\right)^{1/2} x^2\right], \tag{2.22}$$

and the eigenvalue

$$\Omega = \omega(\psi_0) + \frac{1}{2n \mid \nu'(\eta_0) \mid} \left(\frac{\partial^2\omega}{\partial\psi^2} \Big/ \frac{\partial^2\omega}{\partial\eta_0^2}\right)^{1/2}. \tag{2.23}$$

Note that the initial assumption that eigenvalue correction is second order ($\sim 1/n$) is borne out by Eq. (2.23).

An amazing fact is that, although higher order equations are needed to complete the theory, all physically interesting information is obtainable from the lowest order ballooning equation. Therefore, one may be tempted to conclude that all one needs to be concerned about is the lowest order ballooning equation. Such a conclusion, however, should be accepted with caution. There are important restrictions on the applicability of the theory. Firstly, it is valid only at a local extremum of $\omega(\psi)$. Such points, if they exist, are exceptions; in nonideal systems, it may even be impossible to find such points any where on the minor radius [10]. Secondly, the mode must be wide enough compared to the spacing between rational surfaces and narrow enough compared to the equilibrium length scale [16]. The former is required by the $1/\sqrt{n}$ ordered expansion, and the latter is required by the local approximation in Eq. (2.21).

In deriving the ordered equations [Eqs. (2.12), (2.14) and (2.15)], it was assumed that the ψ variation of $f_0(\psi, \eta)$ is on the equilibrium scale. This requires that the parametric dependence of L_0 on ψ be on the equilibrium scale also, which in turn reflects the fact that the fast variations in the fourth argument of $\mathcal{L}$ in Eq. (2.5) must be canceled. The absence of fast variations in

L_0 leads to the so called local translational invariance (or ballooning symmetry) in the eigenfunctions [3, 10, 11]. In order to show this, it is convenient to choose a flux coordinate so that $\nu = \nu(\psi) = q$ [51], and use $x \equiv nq$ as the radial coordinate, so that Eq. (2.4) becomes

$$\widehat{\phi}(x,\eta) = F(x,\eta)e^{-ix(\eta-\eta_0)}. \tag{2.24}$$

We then Fourier decompose $\phi(x,\theta)$ as

$$\phi(x,\theta) = \frac{1}{2\pi}\sum_l \phi_l(x)e^{-il\theta}, \tag{2.25}$$

with

$$\phi_l(x) = \int_0^{2\pi} \phi(x,\theta)e^{il\theta}d\theta. \tag{2.26}$$

Eq. (2.26) is easily calculated with the help of an alternate form of the ballooning transformation [2, 34]

$$\phi(x,\theta) = \sum_N \widehat{\phi}(x,\theta - 2\pi N). \tag{2.27}$$

We have

$$\phi_l(x) = e^{ix\eta_0}\int_{-\infty}^{\infty} F(x,\eta)e^{-i(x-l)\eta}d\eta. \tag{2.28}$$

In lowest order, F is independent of x, and the following relation holds for $\phi_l(x)$

$$\phi_l(x) = e^{i\eta_0}\phi_{l-1}(x-1) = \cdots = e^{im\eta_0}\phi_{l-m}(x-m), \tag{2.29}$$

which is the desired relation for translational invariance. Note that although η is formulated as an extended poloidal angle, it actually determines the local radial structure of $\phi_l(x)$.

It is readily seen from Eqs. (2.25) and (2.28) that ϕ, in lowest order, is a summation of poloidal harmonics (each centered on its own rational surface) with η_0 playing the role of a phase change from one poloidal harmonic to the next. Naturally, the lowest order equation should be one dimensional, since all poloidal harmonics have the same radial structure given by the Fourier transform of $F(\eta)$. Higher order theory essentially implies that, as long as this local structure is not disturbed too much by the global structure, the local eigenvalue is a good estimation of the global eigenvalue.

However, the theory is not as rigorous as it may appear to be. For the summation in Eq. (2.2) (or equivalently Eq. (2.27)) to converge, it is required that $\widehat{\phi}(x,\eta) \to 0$ as $|\eta| \to \infty$. Since the operator $\mathcal{L}(x,\eta)$ is periodic in η, we know from Floquet's theorem that $\widehat{\phi}$ must be of the Floquet form $\widehat{\phi}(x,\eta) = \exp(i\nu\eta)u(x,\eta)$, where u is periodic in η. Therefore, the spectrum of $\mathcal{L}$ must be infinitely degenerate, because any linear combination of a finite number of Floquet states will not converge to zero as $|\eta| \to \infty$ [35].

The infinite degeneracy is easily shown when there is exact translational invariance. In this case, x and ∂_η pairs up in the combination $x - i\partial_\eta$, and the equation for $\widehat{\phi}$ becomes

$$\mathcal{L}\widehat{\phi} = L(\partial_x, x - i\partial_\eta, \eta, \Omega)\widehat{\phi}(x,\eta) = 0. \tag{2.30}$$

Writing $\widehat{\phi} = e^{i\nu\eta}u(x,\eta)$, we have

$$L(\partial_x, x + \nu - i\partial_\eta, \eta, \Omega)u(x,\eta) = 0. \tag{2.31}$$

Suppose the periodic solution to Eq. (2.30) is $\phi(x,\eta)$, then we know from Eq. (2.31) that $\widehat{\phi} = e^{i\nu\eta}\phi(x+\nu,\eta)$ is also a solution with the same eigenvalue.

Thus, in general, we can write

$$\widehat{\phi}(x,\eta) = \int_{-1/2}^{1/2} d\nu A(\nu) e^{i\nu\eta} \phi(x+\nu,\eta), \tag{2.32}$$

where $A(\nu)$ is an arbitrary coefficient.

As long as $A(\nu)$ is continuous and smooth, $\widehat{\phi}$ as given in Eq. (2.32) converges to zero as $|\eta| \to \infty$. Substitution of Eq. (2.32) back into Eq. (2.2) yields the periodic function $\phi(x,\theta)$, irrespective of the shape of $A(\nu)$. This is reminiscent of the fact that the inverse of Eq. (2.2) is not unique. It is by writing $\widehat{\phi}$ in the form of Eq. (2.24) and requiring F to be independent of x that a unique $\widehat{\phi}$ is specified (for which $A(\nu) = 1$).

However, this infinite degeneracy of eigenfunctions can not be shown in general when the translational invariance is only approximate. The construction of $\widehat{\phi}$ as given in Eq. (2.32) satisfies Eq. (2.3) only approximately.

We have shown above in a special case that the inverse of the ballooning transform is not unique. It is also interesting to look at the inverse problem in general. We start by trying to invert Eq. (2.28). First, we write F in terms of its Fourier components

$$F(x,\eta) = \int_{-\infty}^{\infty} f(k,\eta) e^{ikx} dk. \tag{2.33}$$

Multiplying both sides of Eq. (2.28) by $e^{ix\eta'}$ and integrating over x we get

$$\int_{-\infty}^{\infty} f(k,\eta'+k) e^{il(\eta'+k)} dk = \frac{1}{2\pi} \int_{-\infty}^{\infty} \phi_l(x) e^{ix(\eta'-\eta_0)} dx. \tag{2.34}$$

Eq. (2.34) is further reduced by multiplying $e^{-ilk'}$ and sum over l. We have

$$2\pi \sum_N f(k'-\eta'+2\pi N, k'+2\pi N) = \int_{-\infty}^{\infty} dx \phi(x,k') e^{ix(\eta'-\eta_0)}, \tag{2.35}$$

where the identity $\sum_l \exp(ily) = 2\pi \sum_N \delta(y - 2\pi N)$ has been used. It is evident that Eq. (2.35) has infinite many solutions. However, by placing certain restrictions on F, an inverse transform can be defined [34, 36, 37]. If the bandwidth of F is limited to $k \in [-\pi, \pi]$, f is uniquely determined as

$$f(k,\eta) = \frac{1}{2\pi}\int_{-\infty}^{\infty} dx \phi(x,\eta) e^{ix(\eta-k-\eta_0)}, \tag{2.36}$$

where $k \in [-\pi, \pi]$. Substitution back into Eq. (2.33) yields

$$\begin{aligned} F(x,\eta) &= \frac{1}{2\pi}\int_{-\pi}^{\pi} dk \int_{-\infty}^{\infty} dx' \phi(x',\eta) e^{ix'(\eta-k-\eta_0)+ikx} \\ &= \int_{-\infty}^{\infty} dk \frac{\sin \pi k}{\pi k} e^{i(\eta-\eta_0)(x+k)} \phi(x+k,\eta), \end{aligned} \tag{2.37}$$

which is the inversion formula given in Ref. [34]. Although it is always possible to limit the bandwidth of F to $k \in [-\pi, \pi]$ for an arbitrary function $\phi(x, \theta)$, it is the existence of approximate translational invariance that makes this choice natural. Since F is already slow varying with x, limiting its Fourier spectrum to $k \in [-\pi, \pi]$ is hardly an additional constraint. On the other hand, once the inverse transform is defined, the equation for $\widehat{\phi}$ (or equivalently F) should be derived from the inverse transform. Presumably, it is close to Eq. (2.3).

2.2 The 2-D Ballooning Formulation

In this section, we give a general description of our new formulation of the ballooning theory. Instead of using the eikonal represéntation and the conventional ballooning transform [Eq. (2.2)], we build our theory around the 2-D ballooning transform. The 2-D ballooning transform was introduced by Zhang and Mahajan [10] to study nonideal systems in the context of conventional ballooning theory. If we use $x \equiv n(q - q_0)$ (where q is the safety factor,

$q_0 \equiv m/n$ designates some reference rational surface) as the radial coordinate, and write the perturbation Φ as $\Phi(x,\theta,\zeta) \equiv e^{in\zeta - im\theta}\sum_l e^{-il\theta}\phi_l(x)$, the 2-D ballooning transform is defined by

$$\phi_l(x) = \oint d\lambda dk\, e^{ik(x-l)-i\lambda l}\widehat{\phi}(k,\lambda), \tag{2.38}$$

where

$$\oint d\lambda dk \equiv \frac{1}{2\pi}\int_{-\pi}^{\pi} d\lambda \int_{-\infty}^{\infty} dk. \tag{2.39}$$

If $\widehat{\phi}(k,\lambda) = \widehat{\phi}(k,\lambda_0)\delta(\lambda-\lambda_0)$, then Eq. (2.38) becomes

$$\phi_l^0(x) = \int_{-\infty}^{\infty} dk e^{ik(x-l)-i\lambda_0 l}\widehat{\phi}(k,\lambda_0), \tag{2.40}$$

where $\phi_l^0(x)$ clearly satisfies Eq. (2.29) for translational invariance, with λ_0 playing the role of η_0. Since

$$\widehat{\phi}(k,\lambda) = \int d\lambda_0\, \widehat{\phi}(k,\lambda_0)\delta(\lambda-\lambda_0),$$

$\phi_l(x)$ as written in Eq. (2.38) can be thought of as a superposition of these translationally invariant functions.

Unlike the conventional ballooning transform, where the inverse is not uniquely defined in the strict mathematical sense, Eq. (2.38) is a true transform. It is readily inverted by doing an inverse Fourier transform on x and inverting a Fourier series on l. The inversion process shows that although $\widehat{\phi}(x,\lambda)$ needs to be defined only on $\lambda \in [-\pi,\pi]$, it is naturally extended to $\lambda \in (-\infty,\infty)$ by periodic continuation. Therefore by doing the 2-D ballooning transform, a function periodic in θ is replaced by another function periodic in λ. There is no advantage for such a transformation at all, unless the approximate translational invariance can be exploited by the transformed equation. Thus while the

conventional ballooning transform is a result of reconciling the requirements of the eikonal representation and periodicity, the 2-D ballooning transform aims at directly exploiting the translational invariance.

For a formal demonstration of the methodology, it is convenient to use the transformation formula for $\phi(x,\theta) \equiv \sum_l e^{-il\theta}\phi_l(x)$. Substituting $\phi_l(x)$ with Eq. (2.38), we get

$$\phi(x,\theta) = \int_{-\infty}^{\infty} dk e^{ikx}\widehat{\phi}(k,-\theta-k), \tag{2.41}$$

where $\widehat{\phi}(k,\lambda)$ is periodic in λ with periodicity 2π. Replacing k with a new variable $\theta_k = \theta - k$, Eq. (2.41) can be written as

$$\phi(x,\theta) = \int_{-\infty}^{\infty} d\theta_k \widehat{\phi}_D(\theta,\theta_k) e^{ix(\theta-\theta_k)}, \tag{2.42}$$

where $\widehat{\phi}_D(\theta,\theta_k) \equiv \widehat{\phi}(\theta-\theta_k, -2\theta+\theta_k)$ and satisfies the periodicity condition

$$\widehat{\phi}_D(\theta+2\pi,\theta_k+2\pi) = \widehat{\phi}_D(\theta,\theta_k). \tag{2.43}$$

Aside from some difference in notations, Eq. (2.42) is the twisted radial Fourier transform introduced by Dewar [38].

Assume that the equation satisfied by $\phi(x,\theta)$ can be formally written as

$$\mathcal{L}(x,\partial_x;\theta,\partial_\theta)\phi(x,\theta) = \Omega\phi(x,\theta), \tag{2.44}$$

where $\mathcal{L}$ is a self-adjoint operator and Ω is the eigenvalue, the transformed equation is obtained by making the following substitutions

$$\begin{aligned} &x \to i\left(\partial/\partial k - \partial/\partial\lambda\right), \quad \partial/\partial x \to ik, \\ &\theta \to -(\lambda+k), \qquad\qquad \partial/\partial\theta \to -\partial/\partial\lambda. \end{aligned} \tag{2.45}$$

Thus for $\widehat{\phi}(k,\lambda)$ we have

$$\mathcal{L}(i\partial_k - i\partial_\lambda, ik; -(\lambda+k), -\partial_\lambda)\widehat{\phi}(k,\lambda) = \Omega\widehat{\phi}(k,\lambda). \tag{2.46}$$

If the operator $\mathcal{L}$ is translationally invariant, $\partial/\partial\lambda$ would be absent in Eq. (2.46). Violation of translational invariance (or ballooning symmetry) in the system is manifested by the appearance of $\partial/\partial\lambda$ terms in the transformed equation. It's a good idea to expand $\mathcal{L}$ in ascending orders of $\partial/\partial\lambda$ when the ballooning symmetry is only weakly violated. Inserting a formal smallness parameter ϵ in front of $\partial/\partial\lambda$, and carrying the expansion to second order, we obtain

$$\left(L_0 + \epsilon L_1\frac{\partial}{\partial\lambda} + \epsilon^2 L_2\frac{\partial^2}{\partial\lambda^2}\right)\widehat{\phi}(k,\lambda) = \Omega\widehat{\phi}(k,\lambda), \tag{2.47}$$

where

$$\begin{aligned} L_0 &= \mathcal{L}(i\partial_k, ik; -(\lambda+k), 0)\,, \\ L_1 &= \left.\frac{\partial\mathcal{L}[\epsilon]}{\partial\epsilon}\right|_{\epsilon=0} \\ L_2 &= \left.\frac{\partial^2\mathcal{L}[\epsilon]}{\partial\epsilon^2}\right|_{\epsilon=0} \end{aligned} \tag{2.48}$$

Note that the $\partial/\partial\lambda$ terms are associated with the equilibrium scale variations of $\mathcal{L}$, so that $L_1, L_2 \ll L_0$. However, how many terms to include in Eq. (2.47) depends on the specific situation, and convergence of the expansion must be justified on each individual basis.

It is readily seen that the operator L_0 is a differential operator in k only, its λ-dependence being merely parametric. Since L_0 is self-adjoint, its eigenfunctions form a complete set in k space. If the spectrum of L_0 is labeled

by an index p, the eigenfunctions (with corresponding eigenvalues) are defined by

$$L_0\chi_p(k,\lambda) = \omega_p(\lambda)\chi_p(k,\lambda), \tag{2.49}$$

and the relations

$$\langle \chi_{p'} \mid \chi_p \rangle \equiv \int_{-\infty}^{+\infty} dk \chi^*_{p'}(k,\lambda)\chi_p(k,\lambda) = \delta_{p',p}, \tag{2.50}$$

$$\sum_p \chi^*_p(k',\lambda)\chi_p(k,\lambda) = \delta(k-k'), \tag{2.51}$$

express orthonormality and completeness, respectively. We can now expand $\widehat{\phi}$ in terms of χ_p as

$$\widehat{\phi}(k,\lambda) = \sum_p C_p(\lambda)\chi_p(k,\lambda). \tag{2.52}$$

Substituting Eq. (2.52) into Eq. (2.47) and multiplying from the left by $\chi_{p'}$ yields

$$\begin{aligned}\sum_p \Bigg[\langle \chi_{p'} \mid L_2 \mid \chi_p \rangle \frac{d^2 C_p(\lambda)}{d\lambda^2} + \left(\langle \chi_{p'} \mid L_1 \mid \chi_p \rangle + 2\langle \chi_{p'} \mid L_2 \mid \frac{\partial \chi_p}{\partial \lambda} \rangle \right) \frac{dC_p(\lambda)}{d\lambda} \\ + \left(\langle \chi_{p'} \mid L_1 \mid \frac{\partial \chi_p}{\partial \lambda} \rangle + \langle \chi_{p'} \mid L_2 \mid \frac{\partial^2 \chi_p}{\partial \lambda^2} \rangle \right) C_p(\lambda) \Bigg] \\ = \left(\Omega - \omega_{p'}(\lambda)\right) C_{p'}(\lambda),\end{aligned} \tag{2.53}$$

where

$$\langle f \mid L \mid g \rangle \equiv \int_{-\infty}^{+\infty} dk f^* L g.$$

Equation (2.53) is a system of coupled ordinary differential equations with the boundary condition that the $C_p(\lambda)$'s be periodic in λ. If cross coupling

between different p's are small compared to the diagonal terms, an approximate solution is obtainable by considering the diagonal terms only. Such an assumption is often valid when the ballooning symmetry (or translational invariance) is only weakly violated. Under these circumstances equations for $C_p(\lambda)$ are decoupled, and the initial partial differential equation is solved by successively solving two ordinary differential equations. The mode structure is given by the transform of $\widehat{\phi} = C_p(\lambda)\phi_p(k,\lambda)$. As shown in last section, high-n (n is the toroidal mode number) modes in the toroidal plasma have a two length-scale structure: a fast scale for the local structure centered at each rational surface, and a slower scale for the global envelop of the mode. It will become clear in the next chapter that the local structure is contained in ϕ_p, while the global structure is described by $C_p(\lambda)$ (taking place of $A(x)$ in last section). It will also be shown that the procedure outlined here is more general than the conventional theory. Among other things, effects of the cross coupling terms, which are genuinely missing in conventional theory, can be evaluated by perturbation theory (such as in the calculation of continuum damping for the TAE, studied in Chapter 4).

If, on the other hand, the cross coupling terms can not be neglected even in the lowest order approximation, it is impossible to reduce the initial 2-D equation to two ordinary differential equations, and we must solve the system of equations (Eq. (2.53)) simultaneously. Recall that the original partial differential equation is effectively a system of coupled ordinary differential equation in $\phi_l(x)$, it seems we are not making any progress by doing the 2-D ballooning transformation. However, a reduction in the number of coupled equations may still be achievable. Because of the mismatch of different ω_p's, it is likely that

only a small number of C_p's are coupled together. While an analytical theory is not possible, it may still be an effective numerical scheme.

It is interesting to look at the above procedure from another perspective. Let's consider the 2-D transform of $\widehat{\phi}_{p,\lambda'} = \chi_p(k,\lambda)\delta(\lambda-\lambda')$. From Eq. (2.38), we get

$$\begin{aligned}\phi_{p,\lambda'}(x,\theta) &\equiv \sum_l e^{-il\theta}\phi_l^{p,\lambda'}(x) \\ &= \frac{1}{2\pi}\sum_l e^{-il(\theta+\lambda')}\int_{-\infty}^{+\infty} dk\, e^{ik(x-l)}\chi_p(k,\lambda'). \end{aligned} \tag{2.54}$$

It can be shown that

$$\sum_p \int_{-\pi}^{+\pi} d\lambda \phi^*_{p,\lambda}(x',\theta')\phi_{p,\lambda}(x,\theta) = \delta(x-x')\delta(\theta-\theta'). \tag{2.55}$$

Thus $\phi_{p,\lambda}(x,\theta)$, with p labeling the complete set $\chi_p(k,\lambda)$ in k space and λ running from $-\pi$ to π, is complete in the 2-D space (x,θ). An arbitrary function $\phi(x,\theta)$ can then be expanded in terms of $\phi_{p,\lambda}$:

$$\begin{aligned}\phi(x,\theta) &= \sum_p \int d\lambda C_p(\lambda)\phi_{p,\lambda}(x,\theta) \\ &= \sum_l e^{-il\theta}\frac{1}{2\pi}\int_{-\infty}^{+\infty} dk \int_{-\pi}^{+\pi} d\lambda e^{ik(x-l)-il\lambda}\sum_p C_p(\lambda)\chi_p(k,\lambda). \end{aligned} \tag{2.56}$$

It is readily seen that Eq. (2.56) is identical to Eqs. (2.38) and (2.52). Therefore the procedure outlined above is nothing more than the expansion of $\phi(x,\theta)$ in a new set of functions $\phi_{p,\lambda}$, which, in the case of approximate translational invariance, is more convenient than the usual Fourier basis.

For a nonideal system, the operator L_0 is no longer self-adjoint. The expansion procedure is still valid as long as the eigenfunctions of L_0 span the

k space. However, since L_0 often satisfies

$$\int_{-\infty}^{+\infty} dk f L_0 g = \int_{-\infty}^{+\infty} dk g L_0 f, \tag{2.57}$$

for arbitrary functions f and g, the annihilation process is facilitated by multiplying $\chi_p(k,\lambda)$ instead of $\chi_p^*(k,\lambda)$.

Chapter 3

Comparison to Conventional Ballooning Theory

3.1 Introduction

In this chapter, we compare the formulation outlined in Chapter 2 to the conventional ballooning theory of Connor, Hastie and Taylor [1, 2]. For this purpose, the model equations for toroidal drift waves in a tokamak and electrostatic resistive interchange modes in a toroidal pinch (Ref. [16]) will be used. These model equations have been employed by Connor and Taylor [16] to show the relationship between two different descriptions of eigenmodes in a torus. The first are Fourier like modes, contain only a few poloidal harmonics, and highly localized near a particular rational surface. The second, the so called ballooning modes, on the other hand extend over many rational surfaces. It was shown for these simple models that the transition from one to the other is controlled by the variation of a single parameter. And it was concluded that the ballooning approximation is appropriate for drift waves in a tokamak but not for resistive interchange modes in a toroidal pinch.

In Sec. (3.2) we solve the drift wave model by the method outlined in Chapter 2. The results of Ref. [16] are recovered completely. Comparisons with the conventional ballooning theory will be made and it will be shown that our formulation reduces to the conventional theory in a special case.

In Sec. (3.3) the model resistive interchange mode is solved in the same way. While conventional ballooning theory breaks down for this model,

our solution recovers the results of Ref. [16] that were obtained in a completely different way.

Sec. (3.4) is a brief summary. The relationship between the conventional ballooning mode and the "other" ballooning effect is discussed.

3.2 Toroidal Drift Waves

Assume that the perturbed potential is written in the form

$$\varphi(x,\theta) = \phi(x,\theta)\exp[i(n\zeta - m_0\theta) - i\omega t], \tag{3.1}$$

where $x \equiv n(q - q_0)$ is the radial coordinate and $q_0 = m_0/n$ with m_0 defining the central poloidal harmonic. The model equation for toroidal drift waves is

$$\left[\frac{\partial^2}{\partial x^2} - \sigma^2\left(\frac{\partial}{\partial\theta} + ix\right)^2 - \epsilon\left(\cos\theta + is\sin\theta\frac{\partial}{\partial x}\right) - \kappa x^2 - \alpha\right]\phi = 0. \tag{3.2}$$

Here, the first term arises from finite Larmor radius effects and the second term from the ion sound. The third term is the toroidal coupling and the fourth term represents radial variations of the local eigenvalue ($x = 0$ is assumed to be a minimum point). For high-n modes, κ is small ($\sim 1/n$). Definitions for the three parameters σ, ϵ, κ and the relationship of the eigenvalue α to the mode frequency are given in Ref. [16]. The parameter σ^2 is assumed to acquire a small negative imaginary part, so that the mode is bounded in space.

To obtain the transformed equation in ballooning space, we affect the manipulations suggested by Eq. (2.45) [Chapter 2]. Using Eqs. (2.45) and

(2.48), we get

$$L_0 = \left(\sigma^2 - \kappa\right)\frac{\partial^2}{\partial k^2} + k^2 + \epsilon\left[\cos(k+\lambda) + sk\sin(k+\lambda)\right],$$

$$L_1 = 2\kappa\frac{\partial}{\partial k}, \tag{3.3}$$

$$L_2 = -\kappa,$$

implying that the lowest order ballooning equation is

$$(\sigma^2 - \kappa)\frac{\partial^2\chi}{\partial k^2} + k^2\chi + \epsilon\left[\cos(k+\lambda) + sk\sin(k+\lambda)\right]\chi + \widehat{\alpha}(\lambda)\chi = 0. \tag{3.4}$$

If we treat ϵ as a first order small quantity, Eq. (3.4) can be solved perturbatively. The zeroth order equation is a Weber equation and its complete set of eigenvalues and eigenfunctions is given by

$$\widehat{\alpha}_p^{(0)} = -i(2n+1)\sqrt{\sigma^2 - \kappa} \tag{3.5}$$

$$\chi_p^{(0)} = N_p \exp[ik^2/(2\sigma)]H_p(k/\sqrt{i\sigma}), \tag{3.6}$$

where $p = 0, 1, 2, \cdots$, $N_p = (2^p p!\sqrt{i\sigma\pi})^{-1/2}$ is the normalization factor, and H_p is the Hermite polynomial. While the small correction κ has been dropped for the eigenfunctions, it is retained in the eigenvalues for comparison with Ref. [16]. The first order correction for the $p = 0$ mode is

$$\widehat{\alpha}_0^{(1)} = -\int dk\chi_0^{(0)}\left[\epsilon\cos(k+\lambda) + \epsilon sk\sin(k+\lambda)\right]\chi_0^{(0)}$$

$$= -\epsilon\left(1 + \frac{i\sigma s}{2}\right)\exp\left(-\frac{i\sigma}{4}\right)\cos\lambda. \tag{3.7}$$

Perturbative corrections to other eigenvalues can be obtained in the same way. Substitution into Eq. (2.53) yields

$$\kappa\frac{d^2C_p(\lambda)}{d\lambda^2} - 2\kappa\sum_{p'\neq p}\left(\int dk\chi_{p'}^{(0)}\frac{\partial\chi_p^{(0)}}{\partial k}\right)\frac{dC_{p'}(\lambda)}{d\lambda} - (\alpha - \widehat{\alpha}_p(\lambda))C_p(\lambda) = 0, \tag{3.8}$$

where we have changed the roles of p and p'. In deriving Eq. (3.8) only the zeroth order eigenfunctions are used, since matrix elements from perturbative corrections are at least an order ϵ smaller.

If the cross coupling terms can be ignored, the equations decouple, and the lowest eigenmode satisfies

$$\kappa \frac{d^2 C_0(\lambda)}{d\lambda^2} - (\alpha - \widehat{\alpha}_0(\lambda)) C_0(\lambda) = 0. \tag{3.9}$$

Since $\widehat{\alpha}_0(\lambda) = \widehat{\alpha}_0^{(0)} + \widehat{\alpha}_0^{(1)}(\lambda) \approx -i\sigma + i\kappa/(2\sigma) + \widehat{\alpha}_0^{(1)}(\lambda)$, Eq. (3.9) can be rewritten as

$$\frac{d^2 C_0(\lambda)}{d\lambda^2} = (-a + 2b\cos\lambda)\, C_0(\lambda), \tag{3.10}$$

where

$$a = -\frac{\alpha + i\sigma}{\kappa} + \frac{i}{2\sigma}, \tag{3.11}$$

$$b = \frac{\epsilon}{2\kappa}\left(1 + \frac{i\sigma s}{2}\right) \exp\left(\frac{-i\sigma}{4}\right). \tag{3.12}$$

Eq. (3.10) is a Mathieu equation; its periodic solutions are related to the Mathieu functions ce_{2n} and se_{2n}. Periodicity of $C_0(\lambda)$ allows

$$C_0(\lambda) = \sum_l c_l \exp(il\lambda), \tag{3.13}$$

transforming Eq. (3.10) to

$$b(c_{l+1} + c_{l-1}) = (a - l^2) c_l, \tag{3.14}$$

which is identical to Eq.(21) of Ref. [16]. Notice that our approach does not require $b \gg 1$ as does the conventional ballooning theory.

The conventional ballooning theory is recovered when $b \gg 1$. In this case, the potential created by the $\cos\lambda$ term in Eq. (3.10) is very deep, and it is appropriate to replace it by a parabolic potential near an extremum point. For $\lambda \sim 0$, the equation becomes

$$\frac{d^2C(\lambda)}{d\lambda^2} = \left(-a + 2b - b\lambda^2\right) C(\lambda), \tag{3.15}$$

where the subscript 0 has been dropped. The fundamental mode is

$$a = 2b - ib^{1/2}, \tag{3.16}$$

$$C(\lambda) = \exp(ib^{1/2}\lambda^2/2), \tag{3.17}$$

and the Fourier amplitudes c_l are given by

$$c_l = \exp\left(-il^2/(2b^{1/2})\right). \tag{3.18}$$

Since $b \gg 1$, $C(\lambda)$ is very localized at $\lambda \sim 0$, while c_l is broad in l. Back substitution into the 2-D ballooning transform shows that c_l is actually the amplitude of the $m = m_0 + l$ poloidal harmonic. Thus for $b \gg 1$ the eigenmode extends over many rational surfaces with a width $\sim b^{1/4}$, consistent with conventional ballooning theory. This mode has a strong ballooning character with a maximum amplitude at $\theta = 0$, because of the slow variation of c_l with l. It can be easily shown that this c_l-profile conforms to the $A(x)$ profile in the conventional ballooning theory. A similar mode exists with $C(\lambda)$ localized near $\lambda = \pi$, corresponding to a real space structure localized near $\theta = \pi$.

The dropping of cross coupling terms is usually valid when κ is small. Effects of cross coupling can be estimated again by perturbation theory (such a calculation is done in Chapter 4, for the continuum damping of the toroidal

Alfvén eigenmodes). Formally, the correction is of order κ^2 (c.f. Chapter 4). For the drift wave model, cross coupling terms can be safely ignored when σ is of order unity or greater. When σ is comparable to κ, the coefficients in front of the second term of Eq. (3.8) are of order unity, and the cross coupling terms may have a significant effect. However, these effects can only be assessed by numerical works.

3.3 Resisitive Interchange Mode

The model for resistive interchange mode in a large aspect ratio toroidal pinch is

$$\left[\frac{\partial^2}{\partial x^2} + \sigma^2\left(\frac{\partial}{\partial\theta} + ix\right)^2 + i\epsilon s\sin\theta\frac{\partial}{\partial x} - \kappa x^2 - \alpha\right]\phi = 0, \tag{3.19}$$

where ϕ is defined in the same way as in the last section. Definitions for the parameters are given in Ref. [16]. Following Connor and Taylor [16] we consider $\sigma \gg 1$, which is typical in a pinch experiment. In Eq. (3.19) only the geodesic curvature is retained, because for $\sigma \gg 1$ this curvature term dominates over the normal curvature.

The ballooning equation for Eq. (3.19) is

$$\left[\frac{\partial^2}{\partial y^2} - y^2 + \widehat{\epsilon}s\sqrt{\sigma}y\sin(\sqrt{\sigma}y\lambda) - \widetilde{\alpha}\right]\chi = 0, \tag{3.20}$$

where a scale change has been made to facilitate the perturbative solution. The variables are related to the unscaled variables by

$$y = k/\sqrt{\sigma},$$

$$\widehat{\epsilon} = \epsilon/\sigma,$$

and $\tilde{\alpha} = \hat{\alpha}/\sigma$, where $\hat{\alpha}$ is the eigenvalue of the unscaled equation. Treating $\hat{\epsilon}$ as a first order parameter, the zeroth order eigenvalues and eigenfunctions are

$$\tilde{\alpha}_p^{(0)} = -(2n+1), \tag{3.21}$$

$$\chi_p^{(0)} = \exp(-y^2/2) H_p(y), \tag{3.22}$$

where $p = 0, 1, 2, \cdots$ and H_p is the Hermite polynomial.

In the following, we only consider the fundamental mode, i.e. $p = 0$. The first order correction to eigenvalue is

$$\tilde{\alpha}_0^{(1)} = \frac{\hat{\epsilon}\sigma s}{2} \exp(-\sigma/4) \cos\lambda, \tag{3.23}$$

which is exponentially small since σ is large. In order to show the "other" ballooning effect in Ref. [16], we carry out the perturbation theory to second order for the eigenvalue, and to first order for the eigenfunction. The first order eigenfunction can be written as

$$\chi_0^{(1)}(y,\lambda) = \hat{\epsilon} \sum_{p=1}^{\infty} D_p \chi_p^{(0)}(y), \tag{3.24}$$

where the cooeficients D_p are given by

$$D_p = \frac{\int dy \chi_p^{(0)} \left[s\sqrt{\sigma} y \sin(\sqrt{\sigma} y + \lambda) \right] \chi_0^{(0)}}{(\tilde{\alpha}_0^{(0)} - \tilde{\alpha}_p^{(0)}) \int dy (\chi_p^{(0)})^2}. \tag{3.25}$$

Straightforward calculations yields

$$D_p = \begin{cases} \sin\lambda \widehat{D}_p, & p \text{ odd} \\ -\cos\lambda \widehat{D}_p, & p \text{ even} \end{cases} \tag{3.26}$$

with

$$\widehat{D}_p = \frac{(-)^{[\frac{p}{2}]} \sigma^{p/2} \exp(-\sigma/4)(p - \sigma/2) s}{2^{p+1} p p!}, \tag{3.27}$$

where $[x]$ designates the largest integer less or equal to x. The second order correction to the eigenvalue is

$$\begin{aligned}\tilde{\alpha}_0^{(2)} &= \hat{\epsilon}\int dy \chi_0^{(0)}\left[s\sqrt{\sigma}y\sin(\sqrt{\sigma}y+\lambda)\right]\chi_0^{(1)}\Big/\int dy(\chi_0^{(0)})^2 \\ &= \hat{\epsilon}^2 s^2\left(\sum_{N=1}^{\infty}(2N-\sigma/2)^2\frac{(\sigma/2)^{2N}e^{-\sigma/2}}{4N(2N)!}\cos^2\lambda\right. \\ &\quad \left.+\sum_{N=1}^{\infty}(2N-1-\sigma/2)^2\frac{(\sigma/2)^{2N-1}e^{-\sigma/2}}{2(2N-1)(2N-1)!}\sin^2\lambda\right). \qquad (3.28)\end{aligned}$$

In the limit of large σ, the summations can be carried out to give

$$\tilde{\alpha}_0^{(2)} = \hat{\epsilon}^2 s^2/4, \qquad (3.29)$$

which is independent of λ.

Following the steps in the last section, we get

$$\kappa\frac{d^2C_0(\lambda)}{d\lambda^2} = (\alpha - \hat{\alpha}_0(\lambda))C_0(\lambda), \qquad (3.30)$$

where again the cross coupling terms are ignored, and

$$\hat{\alpha}_0(\lambda) = \sigma(\tilde{\alpha}_0^{(0)} + \tilde{\alpha}_0^{(1)} + \tilde{\alpha}_0^{(2)}), \qquad (3.31)$$

is the eigenvalue of the unscaled ballooning equation. Since $\tilde{\alpha}_0^{(1)}$ is exponentially small and $\tilde{\alpha}_0^{(2)}$ is independent of λ, the fundamental mode is given by

$$\begin{aligned}\alpha &= \sigma(\tilde{\alpha}_0^{(0)} + \tilde{\alpha}_0^{(2)}) \\ &= -\sigma + \frac{\epsilon^2 s^2}{4\sigma} \qquad (3.32)\end{aligned}$$

and

$$C_0(\lambda) = \text{constant}. \qquad (3.33)$$

Substitution into the 2-D ballooning transform yields the real space mode structure

$$\phi(x,\theta) = \exp\left(-\frac{\sigma x^2}{2}\right) - \widehat{\epsilon s}\left[\sum_N (-)^N \frac{\sigma^{N/2} e^{-\sigma/4}(N-\sigma/2)}{4NN!2^N} e^{-\sigma(x-1)^2/2} H_N(\sqrt{\sigma}(x-1))\right] e^{-i\theta} - \widehat{\epsilon s}\left[\sum_N \frac{\sigma^{N/2} e^{-\sigma/4}(N-\sigma/2)}{4NN!2^N} e^{-\sigma(x+1)^2/2} H_N(\sqrt{\sigma}(x+1))\right] e^{i\theta}. \quad (3.34)$$

We see that the mode is composed of a central poloidal harmonic with two small side bands. These side bands come from the first order eigenfunction $\chi_0^{(1)}$. The leading order terms in Eq. (3.34) can be summed by the generating function for Hermite polynomials to give

$$\phi(x,\theta) \approx \exp\left(-\frac{\sigma}{2}x^2\right) - \frac{\widehat{\epsilon s}}{4}\exp\left(-\frac{\sigma}{2}x^2\right)\left(e^{i\theta} + e^{-i\theta}\right). \quad (3.35)$$

Note that the side bands are peaked at the same rational surface as the main poloidal harmonic, in agreement with Ref. [16].

In contrast to the toroidal drift waves, which may have extended radial structures spanning many rational surfaces, the resistive interchange mode is highly peaked near a single rational rational surface, consisting of only a few poloidal harmonics. These characters takes the mode out of the range of conventional ballooning theory. By doing a perturbation theory to first order in eigenfunction, two side bands are obtained here for the resistive interchange mode. However, these side bands are localized at the rational surface for the main poloidal harmonic, instead of being centered at their own rational surfaces. This feature was described as the "other" ballooning effect in Ref. [16].

3.4 Summary and Discussions

In this chapter, two model equations are studied in order to illustrate the connection of our ballooning formulation to the conventional ballooning theory. For both models we recover the results of Ref. [16] that were obtained in a different way.

For the toroidal drift wave model, conventional ballooning results are recovered in a special case, i.e. when $b \gg 1$ (b is defined in Sec. (3.2)). The resistive interchange mode exhibits a structure that is highly localized in the radial direction, which makes the conventional ballooning theory inadequate. Instead of showing the conventional ballooning feature, this mode shows "another" type of ballooning effect in which the side band poloidal harmonics are peaked at the same place as the central poloidal harmonic.

These ballooning features, although quite distinct from each other, follow from the same general considerations when we use the 2-D ballooning transform. When the cross coupling terms are ignorable, the real space mode structure is given by the transform of $\widehat{\phi}_p = C_p(\lambda)\chi_p(k,\lambda)$ for a given p. If $\widehat{\phi}_p$ is independent of λ, there would be only one poloidal harmonic. Thus all ballooning features come from the λ-dependence of $\widehat{\phi}_p$. The applicability of conventional ballooning theory (e.g. $b \gg 1$ for the drift wave model) requires $C_p(\lambda)$ to be sharply localized near $\lambda = 0$ or $\lambda = \pi$. This suppresses the effects of λ-dependence in χ_p, and yields an extended radial structure in real space. The real space eigenmode then shows the conventional ballooning feature with a local structure given by the inverse Fourier transform of $\chi_p(k,\lambda_0)$ (where $\lambda_0 = 0, \pi$), and a global envelop given by the Fourier amplitudes of $C_p(\lambda)$, which conforms to the function $A(x)$ in conventional ballooning theory. On the other

hand, when $C_p(\lambda)$ varies slowly with λ, the λ-dependence in χ_p shows up. For the resistive interchange mode, C_0 is independent of λ, and the λ-dependence in χ_p gives rise to the "other" ballooning effect.

In a sense the parameter λ provides a real measure of how strong the toroidal coupling is. When the ballooning eigenvalue is strongly dependent on λ, the mode is expected to be radially wide. On the other hand, when the ballooning eigenvalue is relatively independent of λ, the mode is expected to be more localized. A weak λ-dependence for the ballooning eigenvalues means the poloidal harmonics on different rational surfaces are less correlated, and a small variation from one rational surface to another would be enough to break them up, yielding a mode highly localized in the radial direction.

Chapter 4

Continuum Damping of Ideal Toroidal Alfvén Eigenmodes

4.1 Introduction

In recent years, much effort has been devoted to the study of shear Alfvén waves in a torus, in particular, to the study of toroidicity induced Alfvén eigenmodes (TAE). It was contended that the TAE's, localized within the toroidicity induced gaps of the shear Alfvén continuum, are more likely to be driven unstable by external energy sources, because they are not damped by the phase mixing effect which greatly stablizes shear Alfvén waves in the continuum.

In a deuterium-tritium (D-T) fusion reactor, alpha particles are born at an energy of 3.52MeV, corresponding to a speed higher than the Alfvén speed for typical reactor parameters. Because of the sensitive dependence of fusion reaction rate on plasma temperature, the alpha particle distribution is sharply peaked at the center of the plasma. Plasma instabilities can be induced by this free energy source. In particular, shear Alfvén waves may be driven unstable, since the transit frequency of alpha particle motion is similar to that of shear Alfvén waves. In a sheared magnetic field, the shear Alfvén wave spectrum is a continuum with $(\omega_A)_{min} < \omega < (\omega_A)_{max}$, where ω_A is the local Alfvén frequency [17, 18, 19]. These waves are highly localized in space around $\omega_A(r_0) = \omega$, and are strongly damped by phase mixing. In a toroidal plasma, however, there

are also two types of discrete (and global) modes. The first type, due to the inclusion of equilibrium currents, is called the global Alfvén eigenmode. It lies just below the minimum of the shear Alfvén continuum [39, 40, 41]. Although analysis of this mode in cylindrical geometry showed that it could be driven unstable by wave-particle resonance with super-Alfvénic alpha particles [42], it was shown that in toroidal geometry the mode tends to be stabilized by toroidal coupling [43]. The second type is induced by toroidal coupling, and is called "toroidicity induced Alfvén eigenmode" or the TAE. It lies in the toroidicity induced gaps in the shear Alfvén continuum [9, 20, 44]. (An analog of this mode exists in a straight plasma column due to the ellipticity of the plasma cross section, and is called "ellipticity induced Alfvén eigenmodes" or the EAE [45, 46]). Earlier theories [22, 23] indicated that the TAE is easily excited by alpha particles. It was also shown that even low amplitude TAE's can induce severe alpha particle losses [21]. A proper understanding of the structure and stability of the TAE modes in a modern day tokamak is therefore of great importance, because these modes may limit the confinement time of fusion alpha particles with serious consequences for ignition in a reactor. Similar considerations would hold for experiments with high power neutral beams used for plasma heating or current drive.

Since stability for the TAE is determined by the counterbalance of intrinsic damping and external energy drive, extensive studies have been done to investigate various damping mechanisms. Within the framework of ideal magnetohydrodynamics (MHD), continuum damping (or Alfvén resonance damping) has been identified as one of the more significant damping mechanisms. Berk *et al.* [26] studied the problem in the low-n limit, employing a prescription

of causality for the Alfvén resonance in real space, in analogy to the Landau damping process in velocity space. It was concluded that the continuum damping can significantly reduce the growth rate of alpha particle destabilized TAE modes, and hence lower the wave saturation level. A numerical study based on the same strategy was carried out recently by Chu *et al.* [47]. For the high-n TAE, Rosenbluth *et al.* [14] constructed the eigenmodes by asymptotically matching the solutions across the rational surfaces. The mode structure and complex eigenfrequency (which includes continuum damping) were given by the solution of a three-term recursion relation among coupled poloidal harmonic amplitudes. An extension of this approach to arbitrary-n has been carried out by Berk, Mett and Lindberg [48]. Zonca and Chen, on the other hand, employed a ballooning type approach [15, 49]. The continuum damping rate was obtained by a variational formulation. Finite-β effects were also included in their study [49]. A two-dimensional analytic theory for the TAE was developed recently by Ye, Sedlacek and Mahajan [50], based on an integrodifferential equation formulation. It was shown that the TAEs, instead of being true eigenmodes, were quasimodes associated with zeros of the analytical continuation of the dispersion function onto an unphysical sheet of its Riemann surface.

In this chapter, we present a ballooning theory for the continuum damping of high-n TAEs, based on the theoretical framework described in Chapter 2. Elucidation of the finite lifetime resonant quasimode nature of the TAE is an essential feature of our treatment. Comparing to the approach of Zonca and Chen [49], our lowest order equation (i.e. the so called ballooning equation) is the same as theirs (as it should be for all ballooning type approsches). But treatment for the second dimension is different by the fact that

our λ is a mere parameter while their θ_k is an operator. In our formulation, the continuum damping rate is written explicitly in terms of the coupling between the TAE and shear Alfvén continuum modes. Our analysis also fills in the gaps left by the earlier calculations of Rosenbluth *et al.* [14].

This chapter is organized as follows: In Sec. (4.2), we give a brief derivation of the ideal MHD shear Alfvén wave equation. A perturbation theory for continuum damping of the TAE is given in Sec. (4.3). Detailed calculations are carried out in Secs. (4.4) and (4.5). In Sec. (4.4), the ballooning equation is solved approximately for the disctete as well as the continuum modes near the first gap. The explicit eigenfunctions and coupling matrix elements are given in Sec. (4.5). In Sec. (4.6), we give the numerical results, and compare them with previous calculations, and Sec. (4.7) is devoted to a brief summary and conclusions.

4.2 Shear Alfvén Wave Equation

We consider a circular, axisymmetric, large aspect ratio tokamak with a low beta plasma. The equation for shear Alfvén waves can be easily derived from the reduced MHD equations. The reduced MHD consists of the following equations [51, 52]:

$$\begin{aligned} \frac{1}{v_A^2}\frac{d}{dt}U &= -\nabla_{\|}J - \frac{1}{R_0}[x,p] \\ \frac{1}{c}\frac{\partial\psi}{\partial t} + \nabla_{\|}\varphi &= \frac{\eta c}{4\pi}J \\ \frac{d}{dt}p &= c[\beta,\varphi], \end{aligned} \tag{4.1}$$

where

$$U = c\nabla_\perp^2\varphi, \quad J = \nabla_\perp^2\psi,$$

$$x = (R - R_0)/a,$$

$$\nabla_\| = \mathbf{b}_0 \cdot \nabla - [\psi, \ ], \tag{4.2}$$

$$[f, g] = \mathbf{b}_0 \cdot \nabla f \times \nabla g,$$

$$\frac{d}{dt} = \frac{\partial}{\partial t} + c[\varphi, \ ],$$

and φ is the normalized perturbed scaler potential, ψ is the normalized parallel vector potential, $\mathbf{b}_0$ is a unit vector parallel to the equilibrium magnetic field, $p = 8\pi P_1/B^2$ is the perturbed pressure, $\beta \equiv 8\pi P_0/B^2$ is the equilibrium pressure, R is the distance from the axis of symmetry, R_0 (a) is the major (minor) radius, and c is the speed of light and η is resistivity. For an ideal, low beta plasma, we set $\eta = 0, \beta = 0$. Linearizing the equations yields

$$\frac{1}{v_A^2}\frac{\partial U}{\partial t} = -\nabla_{\|0} J_0 - \nabla_{\|0} J_1 - [\psi_1, J_0], \tag{4.3}$$

$$\frac{1}{c}\frac{\partial \psi_1}{\partial t} + \nabla_{\|0}\varphi = 0, \tag{4.4}$$

where

$$\nabla_{\|0} = \mathbf{b}_0 \cdot \nabla - [\psi_0, \ ], \tag{4.5}$$

and the subscript 0 (1) is used to represent equilibrium (perturbed) quantities. Differentiating Eq. (4.3) with respect to time and substituting in Eq. (4.4), we get

$$\frac{\omega^2}{v_A^2}\nabla_\perp^2\varphi + \nabla_{\|0}\nabla_\perp^2\nabla_{\|0}\varphi + \mathbf{b}_0 \cdot [\nabla_\perp(\nabla_{\|0}\varphi) \times \nabla_\perp J_0] = 0. \tag{4.6}$$

Here we assumed that the time dependence is of the form $e^{-i\omega t}$. The equation can be further simplified by using the canonical coordinates (r, θ, ζ) for a large aspect ratio tokamak, where r is the radial coordinate, θ is the poloidal angle, and ζ is the toroidal angle. These coordinates are defined in terms of the cylindrical coordinates (R, ϕ, Z) as [53]

$$\begin{aligned} R &= R_0 - \Delta + r\cos\theta + \eta(r) r(\cos 2\theta - 1), \\ \phi &= -\zeta, \\ Z &= r\sin\theta + \eta(r) r \sin 2\theta, \end{aligned} \tag{4.7}$$

where $\eta(r) = (r/R_0 + d(\Delta)/dr)/2$, and $\Delta(r)$ is the Shafranov shift. Since the system is axisymmetric, perturbations with different toroidal mode numbers n are decoupled, and we can write φ as

$$\varphi(r, \theta, \zeta) = e^{in\zeta} \sum_m e^{-im\theta} \phi_m(r). \tag{4.8}$$

Substituting this into Eq. (4.6) reduces it to a system of coupled equations. Keeping only nearest neighbor side band coupling, the equations for high n modes can be written as [14]

$$\begin{aligned} \frac{d}{dr}\left[\left(\frac{\omega^2}{v_A^2} - k_{\|m}^2\right)\frac{d\phi_m}{dr}\right] - \frac{m^2}{r^2}\left(\frac{\omega^2}{v_A^2} - k_{\|m}^2\right)\phi_m \\ + \epsilon\frac{\omega^2}{v_A^2}\left(\frac{d^2\phi_{m-1}}{dr^2} + \frac{d^2\phi_{m+1}}{dr^2}\right) = 0, \end{aligned} \tag{4.9}$$

with

$$k_{\|m} = \frac{1}{R_0}\left(n - \frac{m}{q(r)}\right), \epsilon = 5r/2R_0. \tag{4.10}$$

In the limit $\epsilon \to 0$, the poloidal harmonics are decoupled and Eq. (4.9) is essentially the same as the equation for electrostatic oscillations in cold nonuniform plasmas [17, 18]. Equation (4.9) is singular at $\omega^2 = k_{\|m}^2 v_A^2$. It was shown by Barston [17] that this kind of equations exhibit a continuous spectrum determined by the singularities, for Eq. (4.9), it would be $\omega^2 = k_{\|m}^2 v_A^2$. For each frequency ω_0 in the continuum, the corresponding eigenfunction has a singularity at $\omega_0^2 = k_{\|m}^2(r_0) v_A^2(r_0)$. Any smooth excitation, which is a superposition of these normal modes, leads to a noncollective oscillation of the plasma. These excitations are damped by phase mixing, with amplitude decaying algebraically in time. The shear Alfvén spectrum for $n = 3$ without toroidal coupling is schematically shown by the broken lines in Fig. 4.1, with a constant density profile and a q-profile $q = 1 + (r/a)^2$. At certain points, e.g. where $k_{\|m}(r_0) = -k_{\|m+1}(r_0)$, the frequencies for different poloidal harmonics are degenerate. Toroidal coupling (i.e. finite ϵ) resolves this degeneracy and creates gaps (of size $\sim \epsilon$) in the spectrum, as shown by the solid lines in Fig. 4.1. The lowest gap (which we refer to as the first gap) is formed at the degenerate frequency of nearest neighbour poloidal harmonics. In addition, discrete modes (the TAEs) exist inside the gaps. The creation of gaps and existence of the TAE for low-n modes has been shown in Ref. [20]. For high-n modes, this is more conveniently seen in the ballooning space, as will be shown in Sec. (4.4) (c.f. also Ref. [9]).

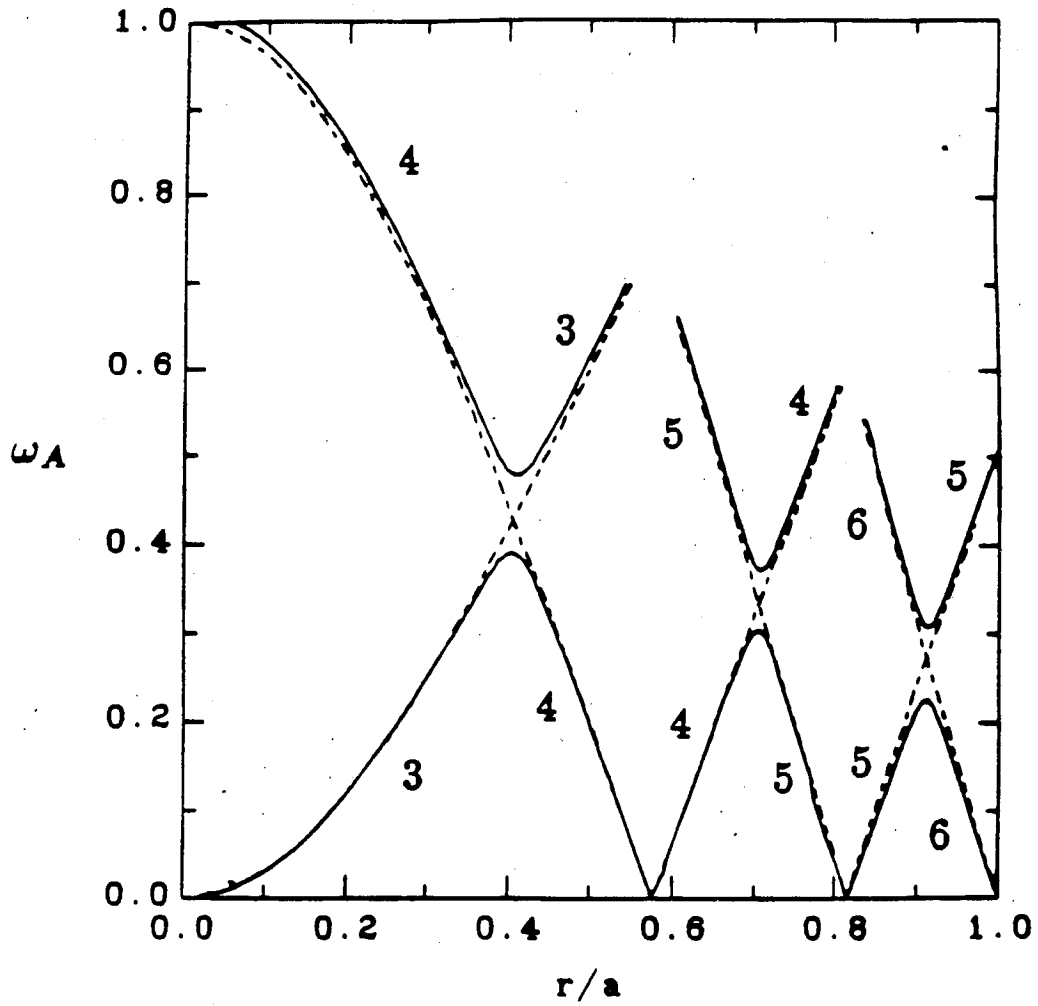

Figure 4.1: Shear Alfvén continuum spectrum for $n = 3$ with constant density profile and safety factor $q = 1+(r/a)^2$. Broken line shows the spectrum without toroidal coupling, for which the mode number m is indicated on the curve. Solid line shows schematically the gap structure created by toroidal coupling. Only the lowest gaps are shown.

4.3 Perturbation Theory for Continuum Damping of the TAE

To put Eq. (4.9) into a form more appropriate for the 2-D ballooning transform, we use $x \equiv n(q - q_0)$ as the radial coordinate, where $q_0 = m/n$ designates some reference rational surface corresponding to the central poloidal harmonic. For Alfvén waves near the first gap, it is convenient to normalize the mode frequancy to the Alfvén frequency $\omega_{A0} \equiv [v_A/(2R_0q)]_{q=q_0}$, which is the degenerate frequency for poloidal harmonics m and $m+1$ when the toroidal coupling is turned off. The first gap is centered around ω_{A0}. Rewriting $\varphi(x,\theta,\zeta)$ as $\varphi = e^{in\zeta - im\theta}\sum_l e^{-il\theta}\phi_l(x)$, Eq. (4.9) can be cast into the form

$$\frac{d}{dx}\left[\frac{\Omega^2 f(x)}{4} - (x-l)^2\right]\frac{d\phi_l}{dx} - \frac{1}{s^2}\left[\frac{\Omega^2 f(x)}{4} - (x-l)^2\right]\phi_l + \frac{\epsilon\Omega^2}{4}\left(\frac{d^2\phi_{l+1}}{dx^2} + \frac{d^2\phi_{l-1}}{dx^2}\right) = 0, \qquad (4.11)$$

where $\Omega \equiv \omega/\omega_{A0}$, $f(x) \equiv \omega_{A0}^2/\omega_A^2$ represents the radial variation of the Alfvén speed, and $s \equiv (d\ln q/d\ln r)_{q=q_0}$ measures the magnetic shear.

For toroidal Alfvén waves near the first gap, it is appropriate to consider $\Omega^2 f(x) \equiv 1 + \epsilon g(x)$ with $g(x) \approx g + 2x/m\hat{\epsilon} + ...$, where $\hat{\epsilon} \equiv \epsilon/[\partial \ln(q^2/v_A^2)/\partial \ln q^2]_{q=q_0}$, and g is the order unity eigenvalue measuring the frequency shift from the center of the gap. Making use of the 2-D ballooning transform

$$\phi_l(x) = \oint d\lambda dk e^{ik(x-l)-i\lambda l}\hat{\Psi}(k,\lambda), \qquad (4.12)$$

and neglecting higher order effects, we obtain an equation in k-λ space

$$\left[\frac{\partial^2}{\partial k^2} + \frac{1+\epsilon g}{4} + \frac{\epsilon}{2}\cos(k+\lambda) - F(k) - \frac{i\epsilon}{2m\hat{\epsilon}}\frac{\partial}{\partial\lambda}\right]\Psi(k,\lambda) = 0 \qquad (4.13)$$

where $\Psi \equiv \widehat{\Psi}\sqrt{1+s^2k^2}$, and $F(k) \equiv s^2/(1+s^2k^2)^2$.

In Eq. (4.11), the ballooning symmetry, i.e., the invariance under the translation $x \to x+1, l \to l+1$, is broken by the radial dependence of $f(x)$. The appearance of the term proportional to $\partial/\partial\lambda$ in Eq. (4.13) is a manifestation of the broken symmetry. Notice that we have neglected higher order symmetry breaking effects [i.e. terms associated with $(x/m)^2$ or $(l/m)^2 \sim (1/m^2)\partial^2/\partial\lambda^2$]. This is valid only if $(1/m)\partial/\partial\lambda$ is *a posteriori* shown to be proportional to a small parameter intrinsic to the problem. In the case of TAE, fortunately, it turns out to be the case: the small parameter being ϵ. Let us define the ballooning operator

$$\mathcal{L}[\lambda] \equiv \frac{\partial^2}{\partial k^2} + \frac{\epsilon}{2}\cos(k+\lambda) - F(k), \tag{4.14}$$

so that Eq. (4.13) can be rewritten as

$$\left[\mathcal{L}[\lambda] + \frac{1+\epsilon g}{4} - \frac{i\epsilon}{2m\widehat{\epsilon}}\frac{\partial}{\partial\lambda}\right]\Psi(k,\lambda) = 0, \tag{4.15}$$

and will be solved perturbatively. The Sturm-Liouville nature of $\mathcal{L}$ guarentees that its eigenfunctions form a complete set in k space. The eigenfunctions are defined by

$$\mathcal{L}[\lambda]\chi_p(k,\lambda) = -\frac{1+\epsilon\widetilde{g}_p(\lambda)}{4}\chi_p(k,\lambda) \tag{4.16}$$

with corresponding eigenvalues $\widetilde{g}_p(\lambda)$. In Eq. (4.16) the λ dependence of various quantities is merely parametric. We can now expand $\Psi(k,\lambda)$ in terms of the complete set χ_p:

$$\Psi(k,\lambda) = \sum_p C_p(\lambda)\chi_p(k,\lambda), \tag{4.17}$$

where the coefficients $C_p(\lambda)$ are projections of $\Psi(k,\lambda)$ onto the base functions $\chi_p(k,\lambda)$. Substituting Eq. (4.17) into Eq. (4.15), and carrying out the standard annihilation procedure (assuming the χ_p's are appropriately normalized), we get

$$\left(H_p - \frac{m\widehat{\epsilon}}{2}g\right) C_p(\lambda) + \sum_{p'\neq p} V_{pp'} C_{p'}(\lambda) = 0, \tag{4.18}$$

where

$$H_p \equiv i\frac{d}{d\lambda} + \frac{m\widehat{\epsilon}}{2}\tilde{g}_p(\lambda) + i\langle\chi_p \mid \frac{\partial\chi_p}{\partial\lambda}\rangle, \tag{4.19}$$

$$V_{pp'} \equiv i\langle\chi_p \mid \frac{\partial\chi_{p'}}{\partial\lambda}\rangle = i\int dk\chi_p^*(k,\lambda)\frac{\partial\chi_{p'}(k,\lambda)}{\partial\lambda}, \tag{4.20}$$

and χ_p^* is the complex conjugate of χ_p.

Before proceeding further, let us comment on the physical significance of the expansion procedure. It is well known that high-n (n is the toroidal number) modes in the toroidal plasma have a two length-scale structure: a fast scale for the local structure of each poloidal harmonic and a slow scale for the coupling between these poloidal harmonics through toroidicity. In the case of a weak violation of the ballooning symmetry, the first term in Eq. (4.18) is dominant. It is easy to confirm that the expansion coefficients $C_p(\lambda)$ in Eq. (4.17) describe the large scale envelop of the mode, while the fine structure of the mode is contained in the functions χ_p's. The term with summation over p' is the coupling between modes of different frequencies. The conventional ballooning theory, while useful in various applications, can not accommodate these coupling terms. However, for the continuum damping of the TAE, it is exactly these terms that are relevant. For large $m\widehat{\epsilon}$, it is appropriate to treat the coupling terms as a perturbation. The lowest order equations are

then decoupled, and the eigenvalues are determined by requiring that $C_p(\lambda)$ be periodic in λ:

$$g^{(0)}_{p,N} = \oint d\lambda \widehat{g}_p(\lambda) - \frac{2N}{m\widehat{\epsilon}}, \tag{4.21}$$

where N is an integer, and

$$\oint d\lambda \equiv \frac{1}{2\pi}\int_{-\pi}^{\pi} d\lambda, \tag{4.22}$$

$$\widehat{g}_p(\lambda) = \widetilde{g}_p(\lambda) + \frac{2i}{m\widehat{\epsilon}}\langle \chi_p \mid \frac{\partial \chi_p}{\partial \lambda}\rangle, \tag{4.23}$$

with corresponding expansion coefficients (determining the eigenfunctions) given by

$$C^{(0)}_{p,N}(\lambda) = \exp\left(-\frac{im\widehat{\epsilon}}{2}\int_0^{\lambda} d\lambda' \left[g^{(0)}_{p,N} - \widehat{g}_p(\lambda')\right]\right). \tag{4.24}$$

Higher order corrections follow from the standard perturbation theory used in quantum mechanics. We readily find that the first order correction to the eigenvalue $g^{(1)}_{p,N} = 0$. The second order correction, given by

$$g^{(2)}_{p,N} = \left(\frac{2}{m\widehat{\epsilon}}\right)^2 \sum_{N'}\sum_{p'\neq p} \frac{\mid \oint d\lambda C^{(0)*}_{p,N}(\lambda) V_{p,p'} C^{(0)}_{p',N'}(\lambda) \mid^2}{g^{(0)}_{p,N} - g^{(0)}_{p',N'}} \tag{4.25}$$

will be used in Sec. (4.5) to calculate the continuum damping rate for the TAE.

4.4 The Spectrum of Ballooning Equation

In Sec. (4.3), we sketched the general methodology to be followed for calculatiing continuum damping. In this section we explicitly solve the ballooning equation [Eq. (4.16)] for its eigenfunctions and eigenvalues. Because the coupling between the TAE and the continuum modes is strongest near the

gap edges, it will suffice to calculate solutions pertinent to the range $\mid \tilde{g} \mid \sim 1$. Noticing that the term F is localised in a region $\mid k \mid \sim 1/s$, we divide the k space into three regions. (I): $k < -1/s$, (II): $\mid k \mid \leq 1/s$, (III): $k > 1/s$. In regions (I) and (III) the F term can be ignored, while in region (II), the toroidal coupling term can be ignored.

The spectrum of Eq. (4.16) becomes clear from a consideration of solutions in the regions (I) and (III). In these regions, it reduces to a Mathieu equation whose spectrum is known to be divided into bands of "stable" and "unstable" solutions. By Floquet's theorem, χ can be written as

$$\chi(k,\lambda) = \exp(i\nu k)u(k,\lambda),$$

where u is periodic in k. Since in outer regions Eq. (4.16) is invariant under spatial reflection $k \to -k, \lambda \to -\lambda$,

$$\chi'(k,\lambda) = \exp(-i\nu k)u(-k,-\lambda)$$

is also a solution with the same value of $\tilde{g}_p$. For a given $\tilde{g}_p$ in a "stable" band, the exponent ν is real, and χ in the outer regions can be generally written as

$$\chi(k,\lambda) = A\exp(i\nu k)u(k,\lambda) + B\exp(-i\nu k)u(-k,-\lambda), \qquad (4.26)$$

where A and B are arbitrary constants. Since we have two free parameters on each side of region (II), it is always possible to find two independent solutions to Eq. (4.16) by matching up the outer solutions through region (II). These solutions form the continuum bands of Eq. (4.16). For $\tilde{g}_p$ in an "unstable" band, the exponent ν is imaginary and the corresponding eigenfunction goes to infinity either at $k \to \infty$ or $k \to -\infty$. These "unstable" bands correspond to

gaps in the spectrum of Eq. (4.16). However, with the presence of the F-term in region (II) inducing a phase change, it becomes possible to match up an evanescent solution in region (I) with an evanescent solution in region (III) for a particular value of $\tilde{g}_p$. This is the so called toroidal Alfvén eigenmode (TAE). The situation is schematically shown in Fig. 4.2 .

For Alfvén waves near the first gap, it is appropriate to write $\chi(k,\lambda)$ in the outer regions as [9]

$$\chi(k,\lambda) = \chi_+ e^{-ik/2} + \chi_- e^{ik/2}, \tag{4.27}$$

where the exponential parts carry the fast variation (of order unity), and χ_+ and χ_- are relatively slow varying. Substitute Eq. (4.27) into Eq. (4.16) and averaging out the fast variations, we obtain the set

$$\chi_+'' - i\chi_+' + \frac{\epsilon}{4}\tilde{g}\chi_+ + \frac{\epsilon}{4}e^{-i\lambda}\chi_- = 0, \tag{4.28}$$

$$\chi_-'' + i\chi_-' + \frac{\epsilon}{4}\tilde{g}\chi_- + \frac{\epsilon}{4}e^{i\lambda}\chi_+ = 0. \tag{4.29}$$

It is apparent that $\chi_\pm' \sim \mathcal{O}(\epsilon)$, and the second order derivatives in Eqs. (4.28) and (4.29) can be neglected. After this simplification, elimination of χ_- from Eqs. (4.28), (4.29) yields

$$\chi_+'' = -\left(\frac{\epsilon}{4}\right)^2 \left(\tilde{g}^2 - 1\right)\chi_+. \tag{4.30}$$

Equation (4.30) clearly reveals that the gap edges are defined by $\tilde{g} = \pm 1$; for $|\,\tilde{g}\,| < 1$, the solution is "unstable", while for $|\,\tilde{g}\,| > 1$ the solution is "stable".

The behavior of $\chi(k,\lambda)$ is considerably more complex in region (II). In general, we can not solve it analytically. But for moderate to large shear, the region (II) is narrow, and for practical purposes we don't need the explicit form

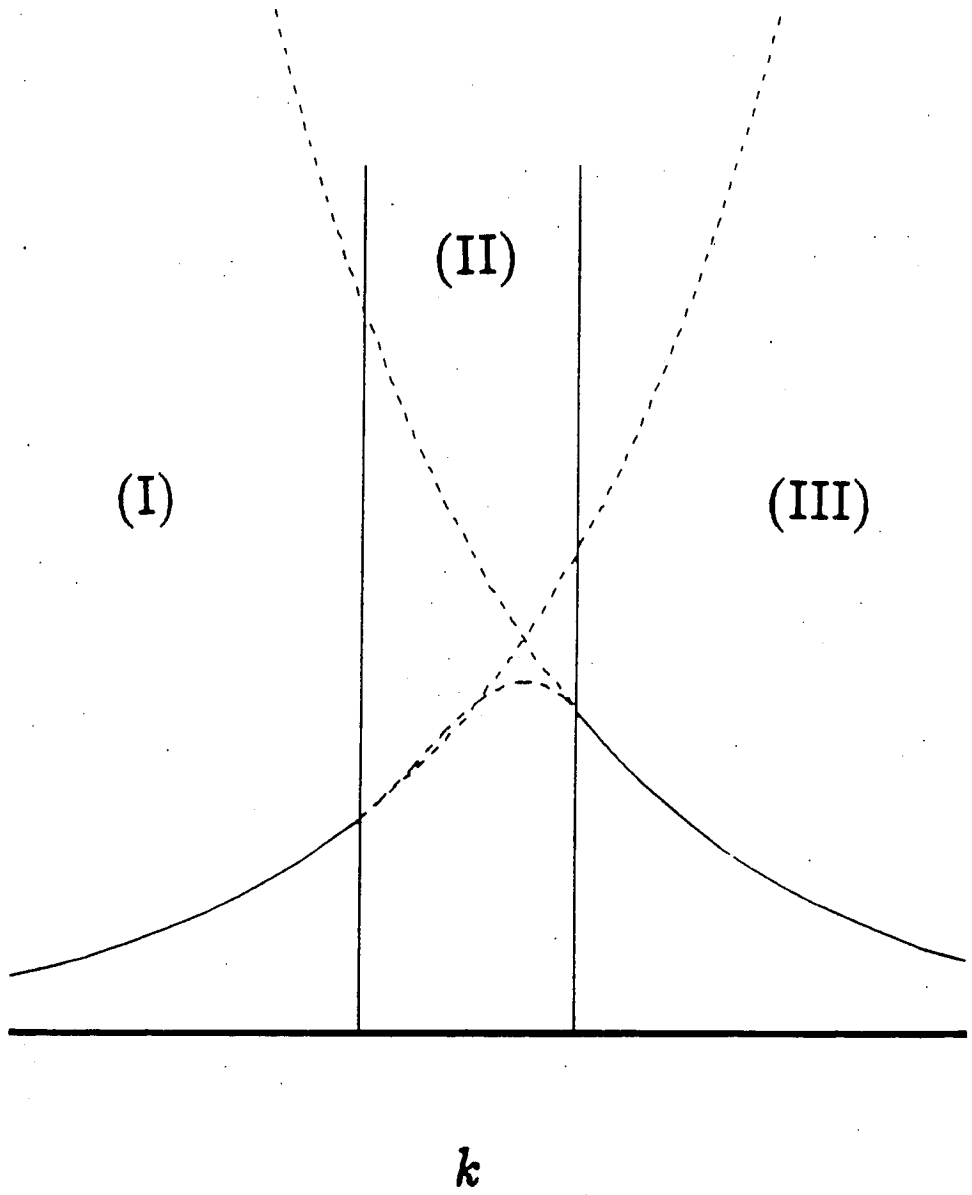

Figure 4.2: Schematic illustration of formation of the TAE. A wave in region (I) that is diverging on the right is matched to a wave in region (III) which diverges on the left, by experiencing a phase change induced by F in region (II).

of $\chi(k,\lambda)$ in this region. The eigenmodes can be approximately obtained by solving Eqs. (4.28) and (4.29) in the outer regions and matching the solutions through region (II). (A similar method was used in Ref. [54]). And the inner product (used to compute quantities of interest) can be conveniently calculated from the outer regions alone,

$$\langle f \mid g \rangle = \left(\int_{-\infty}^{-1/s} dk + \int_{1/s}^{\infty} dk \right) f^*(k,\lambda) g(k,\lambda) \tag{4.31}$$

because the contribution from region (II) is of order ϵ of the contributions from the outer regions.

4.4.1 Matching Rules

In region (II), the F term is dominant, and the toroidal coupling term in Eq. (4.16) can be neglected. Because χ_+ and χ_- are slowly varying, the outer solutions as given in Eq. (4.27) appear to the potential F as plane waves with wavenumber $\widetilde{k} = 1/2$. Thus the effects of potential F on the outer region solutions can be simulated by its scattering parameters of $\widetilde{k} = 1/2$ waves. These parameters are determined by the eigenfunctions of the following equation

$$\left[\frac{\partial^2}{\partial k^2} - F(k) + \frac{1}{4} \right] \chi = 0. \tag{4.32}$$

Since F is symmetric, the eigenfunctions of Eq. (4.32) must have either even or odd parity. In regions (I) and (III), these functions, aside from an arbitrary overall numerical factor, can be written in the following form :

$$\chi_o = \begin{cases} \sin(k/2 - \delta_1); \text{ in region (I)} \\ \\ \sin(k/2 + \delta_1); \text{ in region (III)} \end{cases} \tag{4.33}$$

Table 4.1: Phase shifts (δ_1 and δ_2) for various shear parameters

s	δ_1	δ_2
0.5	−0.2151	−0.7100
0.8	−0.1938	−1.1570
1.0	−0.1761	−1.3013
1.5	−0.1400	−1.4515
2.0	−0.1152	−1.5042

$$\chi_e = \begin{cases} \cos(k/2 - \delta_2); \text{ in region (I)} \\ \\ \cos(k/2 + \delta_2); \text{ in region (III)} \end{cases} \tag{4.34}$$

where $\chi_o(\chi_e)$ has odd (even) parity. These eigenfunctions, and as a result the numerical values of δ_1 and δ_2, are easily obtained with a shooting code. Table 4.1 gives the values of δ_1 and δ_2 for various values of the shear parameter s.

Near the edges of region (II), the slowly varying functions $\chi_\pm$ can be replaced by constants. The general form of the eigenfunction, with $F(k)$ in (II) inducing a phase shift, can be written as:

$$\chi(k,\lambda) = \begin{cases} e^{-ik/2} + C_l e^{ik/2} & \text{in region (I)} \\ \\ \tau(C_r e^{-ik/2} + e^{ik/2}) & \text{in region (III)} \end{cases}$$

up to an overall arbitrary numerical factor. The matching rules relate C_r and τ to C_l. By writing χ as the superposition of χ_e, and χ_o, we get the following expressions for C_r and τ:

$$C_r = \frac{(1 - D_1 D_2) - iD_2(1 + C_l) + iD_1(C_l - 1)}{C_l(1 - D_1 D_2) + iD_2(1 + C_l) + iD_1(C_l - 1)} \tag{4.35}$$

$$\tau = \frac{(1 - D_1 D_2 + iD_1 + iD_2)C_l + i(D_2 - D_1)}{1 + D_1 D_2} \tag{4.36}$$

where $D_1 = \tan\delta_1$, $D_2 = \tan\delta_2$.

4.4.2 Discrete Mode

The discrete mode(s) ($|\ \widetilde{g}\ | < 1$), characterized by evanescent solutions in both regions (I) and (III), can be represented as

$$\chi_+ = \begin{cases} -\tau e^{-i\lambda}\left[\widetilde{g} - i\sqrt{1-\widetilde{g}^2}\right] e^{-\alpha_g k} & \text{in region (III)} \\ e^{\alpha_g k} & \text{in region (I)} \end{cases}, \tag{4.37}$$

where $\alpha_g = \epsilon/4\sqrt{1-\widetilde{g}^2}$. Substituting this back into Eq. (4.28), we obtain:

$$\chi_- = \begin{cases} \tau e^{-\alpha_g k} & \text{in region (III)} \\ e^{i\lambda}\left[i\sqrt{1-\widetilde{g}^2} - \widetilde{g}\right] e^{\alpha_g k} & \text{in region (I)} \end{cases}, \tag{4.38}$$

and consequently

$$C_l = e^{i\lambda}\left(i\sqrt{1-\widetilde{g}^2} - \widetilde{g}\right), \tag{4.39}$$

$$C_r = \frac{e^{-i\lambda}}{-i\sqrt{1-\widetilde{g}^2} - \widetilde{g}}. \tag{4.40}$$

Substituting them into the matching rule [Eq. (4.35)], we get the following equation for $\widetilde{g}$ as a function of λ:

$$-\frac{1 - D_1 D_2}{D_2 - D_1}\sqrt{1-\widetilde{g}^2} + \frac{D_1 + D_2}{D_2 - D_1}\widetilde{g} = \cos\lambda. \tag{4.41}$$

Without loss of generality, we choose the k space mode number $p = 0$ for the discrete mode, and use $g_0(\lambda)$ to denote the solution to Eq. (4.41). Because $|\ g_0(\lambda)\ | < 1$, we can write $g_0(\lambda)$ as:

$$g_0(\lambda) = \cos[\Theta(\lambda)] \tag{4.42}$$

which serves as the definition of Θ as a function of λ. Apparently, we can choose $\Theta \in [0, \pi]$.

Using the expression for C_l [Eq. (4.40)] in Eq. (4.36), we could write

$$\tau(\lambda) = -\tau_R e^{i\lambda}, \tag{4.43}$$

where

$$\tau_R(\lambda) = \frac{(1 - D_1 D_2)\cos\Theta + (D_1 + D_2)\sin\Theta + (D_1 - D_2)\sin\lambda}{1 + D_1 D_2}, \tag{4.44}$$

with $\sin\Theta = \sqrt{1 - g_0^2}$. Thus the normalized eigenfunction for the discrete mode can be written as:

$$\chi_0(k, \lambda) = \left(\chi_+ e^{-ik/2} + \chi_- e^{ik/2}\right)/N_0, \tag{4.45}$$

where χ_+ and χ_- are given in Eqs. (4.37) and (4.38) and

$$N_0 = \left(\frac{4}{\epsilon}\frac{1 + \tau_R^2}{\sqrt{1 - g_0^2}}\right)^{1/2} \tag{4.46}$$

is the normalization factor.

4.4.3 Continuum Modes

The continuum modes ($|\ \tilde{g}\ | > 1$), are oscillatory for large $|\ k\ |$, and can be described by

$$\chi_+ = e^{i\alpha k} + Be^{-i\alpha k} \text{ in regions (I) and (III)}, \tag{4.47}$$

where $\alpha \equiv (\epsilon/4)\sqrt{\tilde{g}^2 - 1}$, and B is an arbitrary constant. Thus the most general form of the eigenfunction in the outer regions can be written as :

$$\begin{aligned}\chi(k, \lambda) = &\left(e^{i\alpha k} + Be^{-i\alpha k}\right) e^{-ik/2} \\ &+ \left[-(\beta + \tilde{g})\, e^{i\alpha k} + B\,(\beta - \tilde{g})\, e^{-i\alpha k}\right] e^{i\lambda + ik/2}\end{aligned} \tag{4.48}$$

in region (I), and

$$\chi(k,\lambda) = \tau\left\{\left(e^{-i\alpha k} + \tilde{B}e^{i\alpha k}\right)e^{ik/2} + \left[-\left(\beta+\tilde{g}\right)e^{-i\alpha k} + \tilde{B}\left(\beta-\tilde{g}\right)e^{i\alpha k}\right]\right\}e^{-i\lambda - ik/2} \tag{4.49}$$

in region (III), where $\beta \equiv \sqrt{\tilde{g}^2-1}$, $\alpha \equiv (\epsilon/4)\beta$, and τ, B and $\tilde{B}$ are constants independent of k.

The matching rules again determine $\tilde{B}$ and τ in terms of B. In general, the continuum eigenfunctions are doubly degenerate, because we have one free parameter B. For definiteness, we choose $\tilde{B} = B$, and use the matching rules to solve B and τ as functions of λ,

$$\begin{aligned} C_l &= \frac{\left[-\left(\beta+\tilde{g}\right)+B\left(\beta-\tilde{g}\right)\right]e^{i\lambda}}{1+B} \\ C_r &= \frac{\left[-\left(\beta+\tilde{g}\right)+B\left(\beta-\tilde{g}\right)\right]e^{-i\lambda}}{1+B}. \end{aligned} \tag{4.50}$$

Substituting these into Eqs. (4.35) and (4.36), we find:

$$B^{\pm} = \frac{2\beta}{\beta-\tilde{g}-Y^{\pm}} - 1, \tag{4.51}$$

where

$$Y^{\pm} = \frac{-i(D_2-D_1)\cos\lambda \pm \sqrt{(1+D_1D_2)^2+(D_2-D_1)^2\sin^2\lambda}}{(1-D_1D_2)+i(D_1+D_2)}, \tag{4.52}$$

and

$$\begin{aligned} \tau^{\pm} &= \frac{(1-D_1D_2+iD_1+iD_2)Ye^{i\lambda}+i(D_2-D_1)}{1+D_1D_2} \\ &= \tau_r^{\pm}e^{i\lambda}, \end{aligned} \tag{4.53}$$

with

$$\tau_r^{\pm} = \frac{(D_2 - D_1)\sin\lambda \pm \sqrt{(1 + D_1 D_2)^2 + (D_2 - D_1)^2 \sin^2\lambda}}{1 + D_1 D_2}.$$

The plus and minus signs give the two linearly independent solutions for the same value of $\tilde{g}$. Noticing that $\tau_r^+ \tau_r^- = -1$, it is straightforward to verify that these two functions are orthogonal to each other (with Eq. (4.31) as the definition for the inner product).

Noticing that $Y^{\pm}$ is a unit vector in the complex plane, we can rewrite $B^{\pm}$ as:

$$B^{\pm} = (\beta + \tilde{g}) e^{i\Theta_{\pm}}, \tag{4.54}$$

which in turn defines the functions $\Theta_{\pm}$. The continuum eigenfunctions can now be written in a more convenient way: in terms of the functions $\Theta_{\pm}$. The normalized eigenfunctions for the continuum modes are:

$$\chi_{\tilde{g}}^{(+)}(k,\lambda) = \begin{cases} (1/N_c)\left\{\left[e^{i\alpha k} + (\beta+\tilde{g})\, e^{i\Theta_+ - i\alpha k}\right] e^{-ik/2} \right. \\ \quad \left. + \left[-(\beta+\tilde{g})\, e^{i\alpha k} - e^{i\Theta_+ - i\alpha k}\right] e^{i\lambda + ik/2}\right\} \text{ in region (I)} \\ (\tau_r/N_c)\left\{\left[e^{-i\alpha k} + (\beta+\tilde{g})\, e^{i\Theta_+ + i\alpha k}\right] e^{ik/2 + i\lambda} \right. \\ \quad \left. + \left[-(\beta+\tilde{g})\, e^{-i\alpha k} - e^{i\Theta_+ + i\alpha k}\right] e^{-ik/2}\right\} \quad \text{in region (III)} \end{cases} \tag{4.55}$$

$$\chi_{\tilde{g}}^{(-)}(k,\lambda) = \begin{cases} -(\tau_r/N_c)\left\{\left[e^{i\alpha k} + (\beta+\tilde{g})\, e^{i\Theta_- - i\alpha k}\right] e^{-ik/2} \right. \\ \quad \left. + \left[-(\beta+\tilde{g})\, e^{i\alpha k} - e^{i\Theta_- - i\alpha k}\right] e^{i\lambda + ik/2}\right\} \quad \text{in region (I)} \\ (1/N_c)\left\{\left[e^{-i\alpha k} + (\beta+\tilde{g})\, e^{i\Theta_- + i\alpha k}\right] e^{ik/2 + i\lambda} \right. \\ \quad \left. + \left[-(\beta+\tilde{g})\, e^{-i\alpha k} - e^{i\Theta_- + i\alpha k}\right] e^{-ik/2}\right\} \quad \text{in region (III)} \end{cases} \tag{4.56}$$

where the normalization constant $N_c = \sqrt{4\pi(1+\tau_r^2)\tilde{g}(\beta+\tilde{g})}$. These eigenfunctions are δ-function normalized with respect to the variable $\alpha = \epsilon/4\sqrt{\tilde{g}^2 - 1}$.

For the calculation of the coupling matrix elements, we shall use a more convenient set of base functions $\widetilde{\chi}_{\tilde{g}}^{(\pm)}$:

$$\widetilde{\chi}_{\tilde{g}}^{(\pm)} = ie^{-i\Theta_{\pm}/2}\chi_{\tilde{g}}^{(\pm)}. \tag{4.57}$$

It's easy to see that $\widetilde{\chi}_{\tilde{g}}^{(\pm)}$ equals a real normalized function times a phase factor $e^{i\lambda/2}$. This property greatly simplifies the calculations.

4.5 Calculations in the Second Dimension

In order to use the perturbation theory expressions in section (II), we need to calculate the coupling matrix elements. For the self-coupling of the discrete mode, this is straightforward. The discrete eigenfunction given by Eq. (4.45) can be put in the form

$$\chi_0(k,\lambda) = -ie^{-i(\Theta-\lambda)/2}\widetilde{\chi}_0(k,\lambda), \tag{4.58}$$

where $\widetilde{\chi}_0$ is a real and normalized function. Thus the self-coupling for the discrete mode is

$$\begin{aligned}\langle\chi_0 \mid \frac{\partial\chi_0}{\partial\lambda}\rangle &= \langle\widetilde{\chi}_0 \mid \frac{\partial\widetilde{\chi}_0}{\partial\lambda}\rangle - \frac{i}{2}\frac{\partial(\Theta-\lambda)}{\partial\lambda} \\ &= -\frac{i}{2}\left(\frac{\partial\Theta}{\partial\lambda} - 1\right),\end{aligned} \tag{4.59}$$

which, when substituted into Eqs. (4.21) and (4.24), yields

$$g_{0,N}^{(0)} = -\frac{2}{m\widehat{\epsilon}}\left(N+\frac{1}{2}\right) + \overline{\cos\Theta}, \tag{4.60}$$

and

$$\begin{aligned}C_{0,N}^{(0)}(\lambda) &= \exp\left(\frac{i\Theta}{2} + iN\lambda + i\frac{m\widehat{\epsilon}}{2}\int_0^{\lambda} d\lambda'\left(\cos\Theta(\lambda') - \overline{\cos\Theta}\right)\right) \\ &= e^{iN\lambda}C_{0,0}^{(0)}(\lambda),\end{aligned} \tag{4.61}$$

with

$$\overline{\cos\Theta} = \oint \cos\Theta d\lambda. \tag{4.62}$$

The interesting point here is that although we did the Fourier expansion assuming the TAE mode is centered about a rational surface, the quantization rule [Eq. (4.60)] carries the mode to a place in between two rational surfaces — the place where the TAE should be located. This is seen most clearly in the small shear limit, where the function $\Theta(\lambda)$ approaches a constant, the mode resides half way in between the two mode rational surfaces, giving the usual single gap structure [c.f. Chapter 5]. The corresponding real space mode structure for the TAE is:

$$\begin{aligned}\Phi^{(0)}_{0,N}(x,\theta) &= \oint d\lambda C^{(0)}_{0,N}(\lambda) \sum_l e^{-il(\theta+\lambda)} \int dk e^{ik(x-l)} \frac{\chi_0(k,\lambda)}{\sqrt{1+s^2k^2}} \\ &= e^{-iN\theta} \oint d\lambda C^{(0)}_{0,N}(\lambda) \sum_l e^{-il(\theta+\lambda)} \int dk e^{ik(x-l-N)} \frac{\chi_0(k,\lambda)}{\sqrt{1+s^2k^2}} \\ &= e^{-iN\theta} \Phi^{(0)}_{0,0}(x-N,\theta). \end{aligned} \tag{4.63}$$

Thus the significance of the quantum number N is to shift the $N=0$ mode by N rational surfaces, which is equivalent to do the mode expansion at another rational surface with $m' = m + N$ and take the $N' = 0$ mode there. Of course this is a consequence of the symmetry properties peculiar to our present model, i.e. a consequence of the linear profile assumption for the local Alfvén speed. One point of caution in practice is that N can not be too large lest the mode is carried out of the region of validity of the origional assumptions.

The calculations for the continuum modes in the second dimension is a little bit more complicated. Because these modes are degenerate, any orthonormal set of functions, $\tilde{\chi}^{(\pm)}_{\bar{g}}$ as well as any linear combination of them can be

used as the base functions. This causes some uncertainty in the cross coupling terms. For definiteness, we need to include the coupling term between $\tilde{\chi}_{\tilde{g}}^{(+)}$ and $\tilde{\chi}_{\tilde{g}}^{(-)}$ in the lowest order continuum equations. Thus we have

$$\left[\frac{d}{d\lambda} + \langle\tilde{\chi}_{\tilde{g}}^{(+)} \mid \frac{\partial\tilde{\chi}_{\tilde{g}}^{(+)}}{\partial\lambda}\rangle + i\frac{m\widehat{\epsilon}}{2}(g-\tilde{g})\right] C_{(+)}(\lambda)$$

$$= -\langle\tilde{\chi}_{\tilde{g}}^{(+)} \mid \frac{\partial\tilde{\chi}_{\tilde{g}}^{(-)}}{\partial\lambda}\rangle C_{(-)}(\lambda) \quad (4.64)$$

$$\left[\frac{d}{d\lambda} + \langle\tilde{\chi}_{\tilde{g}}^{(-)} \mid \frac{\partial\tilde{\chi}_{\tilde{g}}^{(-)}}{\partial\lambda}\rangle + i\frac{m\widehat{\epsilon}}{2}(g-\tilde{g})\right] C_{(-)}(\lambda)$$

$$= -\langle\tilde{\chi}_{\tilde{g}}^{(-)} \mid \frac{\partial\tilde{\chi}_{\tilde{g}}^{(+)}}{\partial\lambda}\rangle C_{(+)}(\lambda) \quad (4.65)$$

as the zeroth order equation for the continuum modes.

To get around the complexity of solving Eqs. (4.64) and (4.65) simultaniously, we look for a unitary transfomations from $\tilde{\chi}_{\tilde{g}}^{(\pm)}$ to a new set $\psi_{\tilde{g}}^{(\pm)}$ such that the cross coupling term in the new representation is zero, i.e.

$$\langle\psi_{\tilde{g}}^{(+)} \mid \frac{\partial\psi_{\tilde{g}}^{(-)}}{\partial\lambda}\rangle = \langle\psi_{\tilde{g}}^{(-)} \mid \frac{\partial\psi_{\tilde{g}}^{(+)}}{\partial\lambda}\rangle = 0. \quad (4.66)$$

Without loss of generality, we can write

$$\psi_{\tilde{g}}^{(+)} = e^{i\xi_1}\sin\gamma\,\tilde{\chi}_{\tilde{g}}^{(+)} + e^{i\xi_2}\cos\gamma\,\tilde{\chi}_{\tilde{g}}^{(-)}$$

$$\psi_{\tilde{g}}^{(-)} = e^{i\xi_3}\cos\gamma\,\tilde{\chi}_{\tilde{g}}^{(+)} + e^{i\xi_4}\sin\gamma\,\tilde{\chi}_{\tilde{g}}^{(-)}, \quad (4.67)$$

where $\gamma \in [0, \pi/2]$, $(\xi_1 - \xi_2) - (\xi_3 - \xi_4) = \pi$, γ and ξ_i's are arbitrary periodic functions of λ. Substituting Eq. (4.67) into Eq. (4.66) yields

$$\frac{dz}{d\lambda} = \left(\langle \tilde{\chi}_{\tilde{g}}^{(+)} \mid \frac{\partial \tilde{\chi}_{\tilde{g}}^{(+)}}{\partial \lambda} \rangle - \langle \tilde{\chi}_{\tilde{g}}^{(-)} \mid \frac{\partial \tilde{\chi}_{\tilde{g}}^{(-)}}{\partial \lambda} \rangle \right) z$$

$$-z^2 \langle \tilde{\chi}_{\tilde{g}}^{+} \mid \frac{\partial \tilde{\chi}_{\tilde{g}}^{-}}{\partial \lambda} \rangle - \langle \tilde{\chi}_{\tilde{g}}^{+} \mid \frac{\partial \tilde{\chi}_{\tilde{g}}^{-}}{\partial \lambda} \rangle^* \tag{4.68}$$

where $z = e^{-i(\xi_1 - \xi_2)} \tan\gamma$. Substituting $\tilde{\chi}_{\tilde{g}}^{(\pm)}$ given by Eq. (4.57) into the above equation, we find that the first term is zero, the other two terms are real. Therefore, $z = \pm i$ are the exact solutions of Eq. (4.68). Without loss of generality, we choose $z = i$. The new set of base functions are

$$\psi_{\tilde{g}}^{(\pm)}(k, \lambda) = \frac{1}{\sqrt{2}} \left(\tilde{\chi}_{\tilde{g}}^{(+)} \mp i \tilde{\chi}_{\tilde{g}}^{(-)} \right). \tag{4.69}$$

In the new basis, it is straightforward to calculate the self-coupling matrix elements:

$$\langle \psi_{\tilde{g}}^{(+)} \mid \frac{\partial \psi_{\tilde{g}}^{(+)}}{\partial \lambda} \rangle = \frac{i}{2} + i \langle \tilde{\chi}_{\tilde{g}}^{(-)} \mid \frac{\partial \tilde{\chi}_{\tilde{g}}^{(+)}}{\partial \lambda} \rangle \tag{4.70}$$

$$\langle \psi_{\tilde{g}}^{(-)} \mid \frac{\partial \psi_{\tilde{g}}^{(-)}}{\partial \lambda} \rangle = \frac{i}{2} - i \langle \tilde{\chi}_{\tilde{g}}^{(-)} \mid \frac{\partial \tilde{\chi}_{\tilde{g}}^{(+)}}{\partial \lambda} \rangle, \tag{4.71}$$

where

$$\langle \tilde{\chi}_{\tilde{g}}^{(-)} \mid \frac{\partial \tilde{\chi}_{\tilde{g}}^{(+)}}{\partial \lambda} \rangle = S(\lambda) \delta(\alpha - \alpha'), \tag{4.72}$$

$$S(\lambda) = \tau_r \frac{\frac{(D_2 - D_1)\cos\lambda}{\sqrt{(1+D_1 D_2)^2 + (D_2 - D_1)^2 \sin^2\lambda}} \tilde{g} \cos\left(\frac{\Theta_+ - \Theta_-}{2}\right) - \beta \sin\left(\frac{\Theta_+ - \Theta_-}{2}\right)}{(1 + \tau_r^2)\tilde{g}}, \tag{4.73}$$

and $\alpha \equiv \epsilon / 4\sqrt{\tilde{g}^2 - 1}$.

Substituting these into Eqs. (4.21), (4.24) for the zeroth order eigenvalue and eigenfunction, we get

$$g_{\tilde{g},N}^{(0)\pm} = \tilde{g} - \frac{2N+1}{m\hat{\epsilon}} \mp \frac{2}{m\hat{\epsilon}}\overline{S(\lambda)} \tag{4.74}$$

$$C_{\tilde{g},N}^{(0)\pm}(\lambda) = \exp\left[iN\lambda \mp i\int_0^\lambda d\lambda' \left(\overline{S(\lambda)} - S(\lambda')\right)\right] \tag{4.75}$$

where

$$\overline{S(\lambda)} = \oint d\lambda S(\lambda). \tag{4.76}$$

Eq. (4.25) can now be used to calculate the continuum damping. We need only consider the $N = 0$ case. Because the spectrum is a continuum except for the discrete mode, the summation over p' should be replaced with an integral

$$g_{0,0}^{(2)} = \left(\frac{2}{m\tilde{\epsilon}}\right)^2 \sum_N \int d\tilde{g} \frac{|\oint d\lambda C_{\tilde{g},N}^{*(0)}(\lambda) V_{0,\tilde{g}}(\lambda) C_{0,0}^{(0)}(\lambda)|^2}{g_{0,0}^{(0)} - g_{\tilde{g},N}^{(0)}}, \tag{4.77}$$

where $|\tilde{g}| > 1$ and the ballooning eigenfunctions are δ-function normalized with respect to $\tilde{g}$. For the eigenfunctions given by Eq. (4.57), where they are δ-function normalized with respect to the variable $\alpha = (\epsilon/4)\sqrt{\tilde{g}^2 - 1}$, Eq. (4.77) should be changed to

$$g_{0,0}^{(2)} = \left(\frac{2}{m\tilde{\epsilon}}\right)^2 \sum_N \int d\tilde{g} \frac{\epsilon}{4} \frac{\tilde{g}}{\sqrt{\tilde{g}^2 - 1}} \frac{|\oint d\lambda C_{\tilde{g},N}^{*(0)}(\lambda) V_{0,\tilde{g}}(\lambda) C_{0,0}^{(0)}(\lambda)|^2}{g_{0,0}^{(0)} - g_{\tilde{g},N}^{(0)}}. \tag{4.78}$$

Notice that the integrand in Eq. (4.78) has a first order singularity at the resonance points $g_{\tilde{g},N}^{(0)} = g_{0,0}^{(0)}$. The contour of the integral should be deformed as in the Landau-damping problem. If positive real frequency is

adpoted, the correct contour is determined by giving the variable $g^{(0)}_{0,0}$ a small positive imaginary part. Thus

$$\mathrm{Im}\left[g^{(2)}_{0,0}\right] = -\frac{4\pi}{(m\widehat{\epsilon})^2}\frac{\epsilon}{4}\sum_N \frac{\widetilde{g}_N}{\sqrt{\widetilde{g}_N^2-1}} \mid \oint d\lambda C^{*(0)}_{\widetilde{g}_N,N}(\lambda) V_{0,\widetilde{g}_N}(\lambda) C^{(0)}_{0,0}(\lambda) \mid^2, \quad (4.79)$$

where $\widetilde{g}_N$ is the root of $g^{(0)}_{\widetilde{g},N} = g^{(0)}_{0,0}$.

The explicit forms of the coupling matrix elements between the discrete and continuum modes are given in Appendix A.

4.6 Numerical Results

The continuum damping rate for various shear are obtained by numerically evaluating the right hand side of Eq. (4.79). Results for $s = 0.5, 1.0, 1.5$ and $s = 2.0$ are shown in Figs. 4.3 and 4.4. In all cases, the damping rate changes rapidly with the variation of the parameter $m\widehat{\epsilon}$, which specifies the slope of linear profile for the local Alfvén speed. This is because the coupling between the TAE and the continuum modes is concentrated near the gap edges, i.e. the maximum absolute value of $V_{0,\widetilde{g}}(\lambda)$ appears at some place $\mid \widetilde{g} \mid \sim 1+\varepsilon$. When $m\widehat{\epsilon}$ is changed, it moves the TAE in and out of this region of maximum coupling, causing the dampig rate to go higher and lower. The situation is illustrated in Figs. 4.5 and 4.6 for $s = 0.5$. The TAE considered is centered at $x = 1/2$. For $m\widehat{\epsilon} = 8.0$, the TAE frequency intersects the continuum two gaps to the left, near the top of edge, thus experiencing large damping. While for $m\widehat{\epsilon} = 9.5$, the TAE just missed the second gap and still deep in the third gap, so that the damping is near minimum. When s becomes larger, this area of maximum coupling becomes narrower, thus the damping rate oscillates more violently with $m\widehat{\epsilon}$. It is readily observable that the continuum damping rate

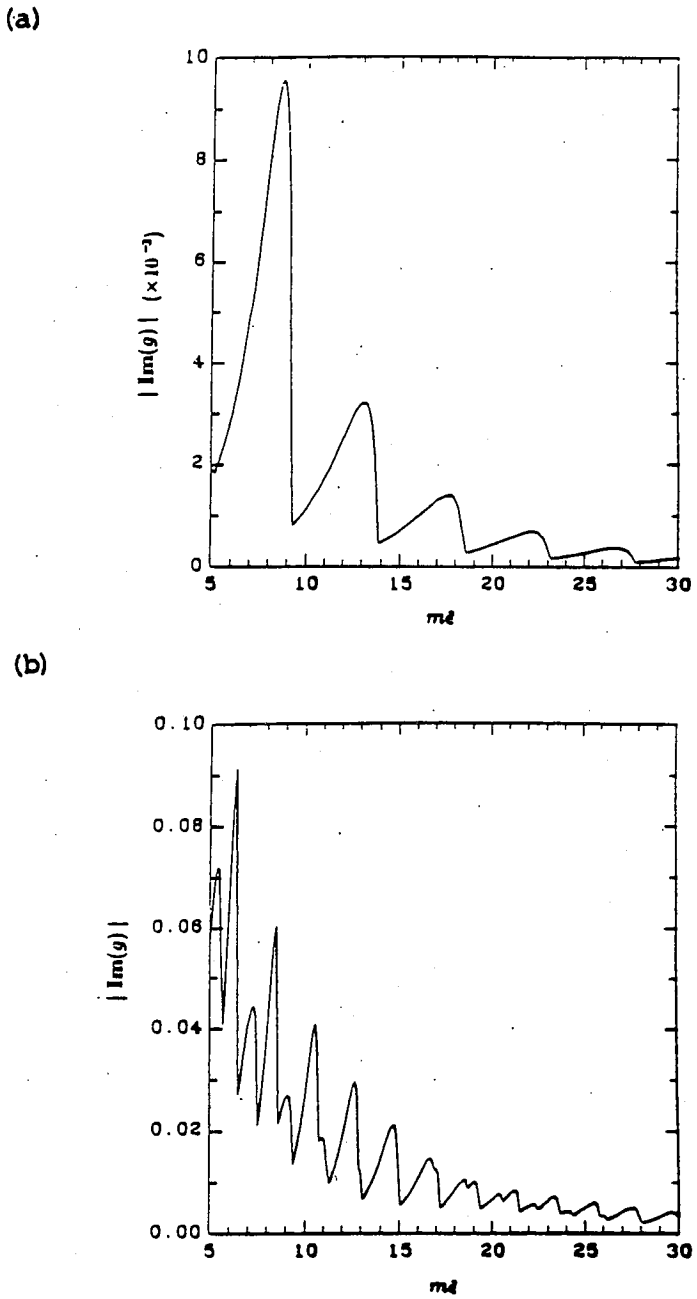

Figure 4.3: Continuum damping rate as a function of $m\hat{\epsilon}$ for shear parameters (a): $s = 0.5$, (b): $s = 1.0$.

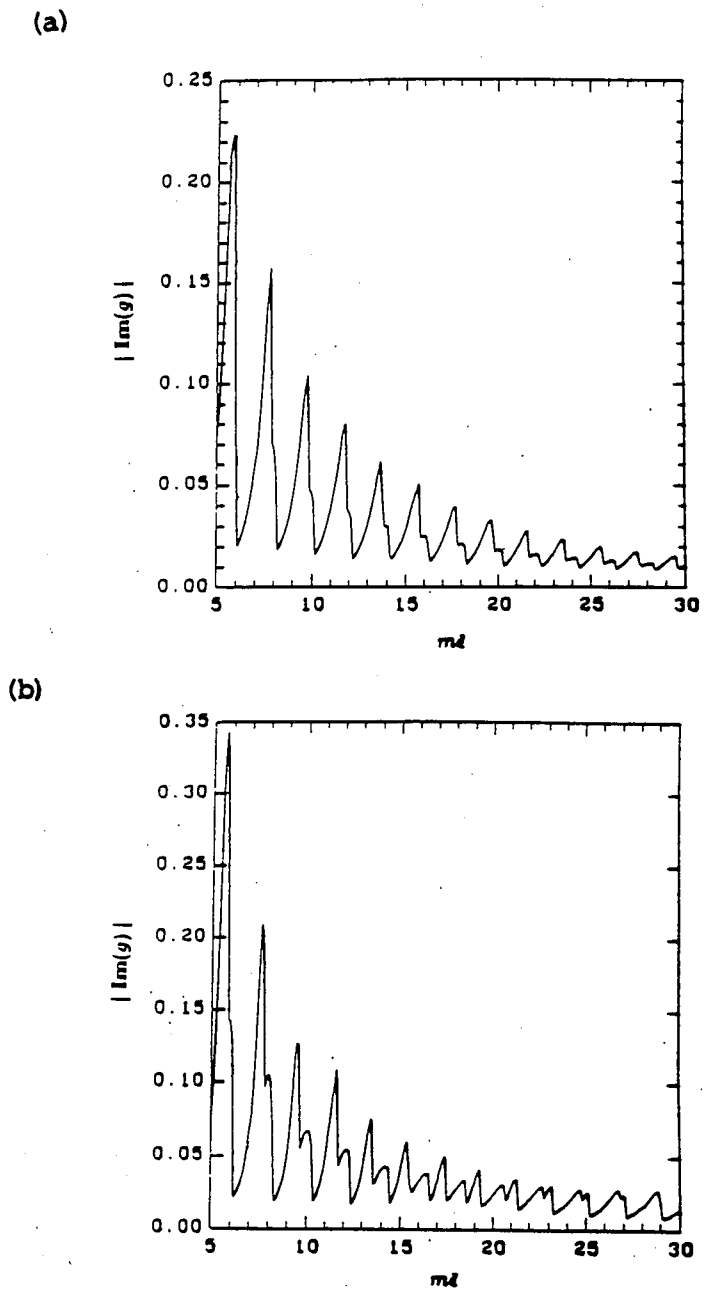

Figure 4.4: Continuum damping rate as a function of $m\hat{\epsilon}$ for shear parameters (a): $s = 1.5$, (b): $s = 2.0$

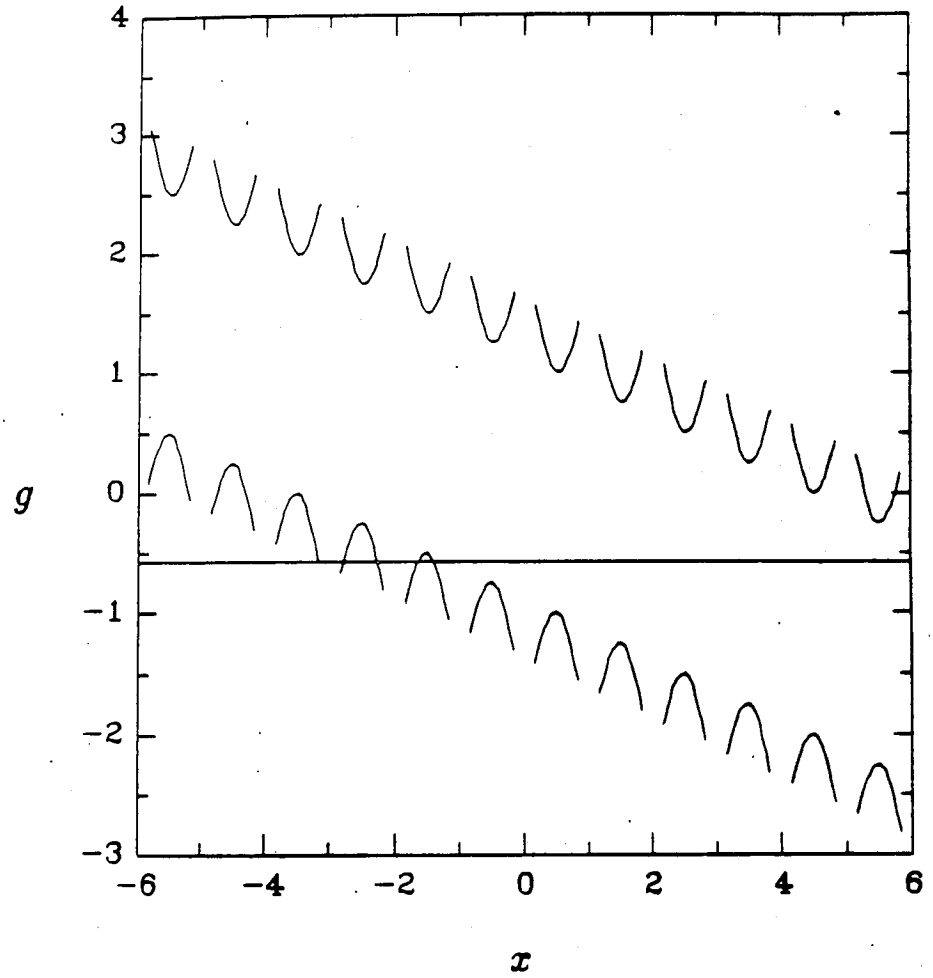

Figure 4.5: Gap structure with TAE frequency for $s = 0.5$ and $m\hat{\epsilon} = 8.0$. The curves represent the continuum spectrum, the straight line at $g = -0.57$ represents the TAE frequency.

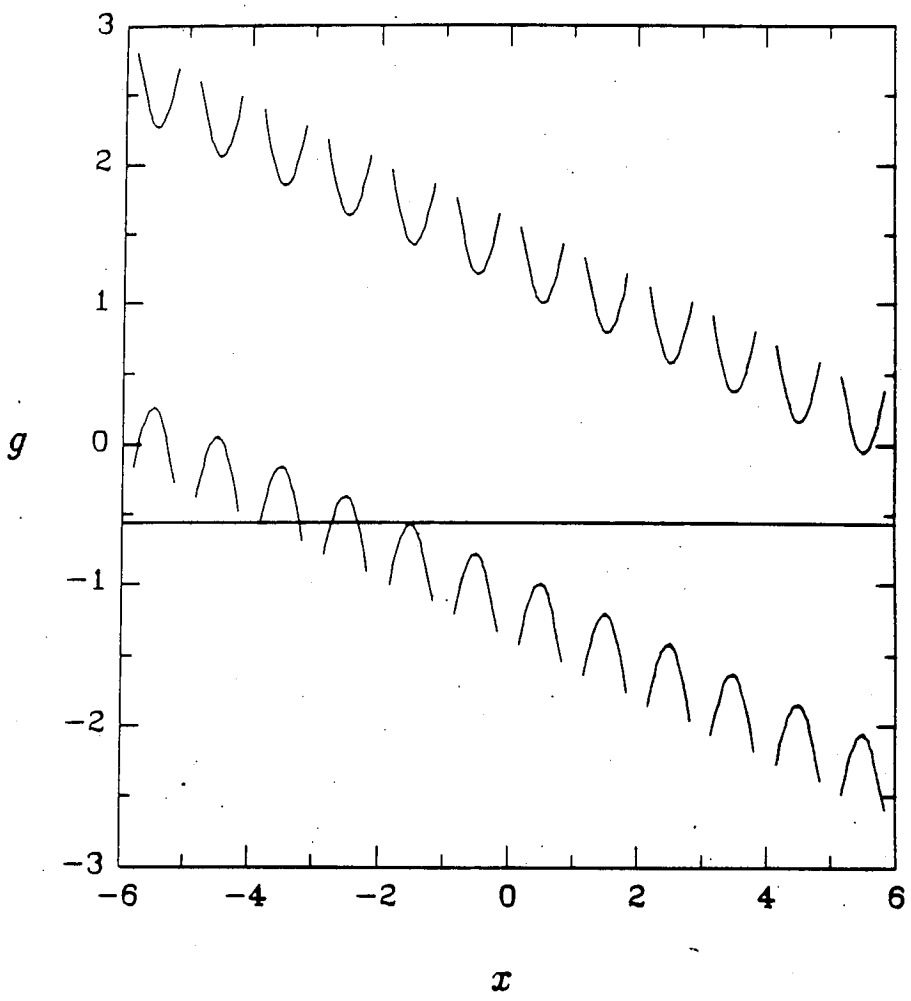

Figure 4.6: Gap structure with TAE frequency for $s = 0.5$ and $m\hat{\epsilon} = 9.5$. The curves represent the continuum spectrum, the straight line at $g = -0.57$ represents the TAE frequency.

grows with larger shear. This increase comes from two factors: first, the radial extent of the TAE increases with shear, causing more resonance points to come into the effective range of the TAE; second, the maximum value of the coupling matrix element $V_{0,\bar{g}}(\lambda)$ also increases with shear.

Figure 4.7 compares our present calculations with that of Ref. [14] for the case $s = 0.8$. The results are in good agreement, except that in the latter there are regions in $m\hat{\epsilon}$ where solutions could not be found. It is clear that our approach yields the damping as a continuous function of $m\hat{\epsilon}$: there are no missing intervals where the roots could not be found. The regions [in $m\hat{\epsilon}$] of rapid variation and turning around of the damping rate coincide with the intervals which could not be handled by the methods of Ref. [14].

4.7 Summary and Conclusions

The continuum damping effects on the toroidal Alfvén eigenmodes are calculated by using a ballooning approach. The origional 2-D eigenvalue problem is converted into an eigenvalue problem in the usual ballooning space and a set of first order differential equations for the global structure and eigenvalue in a second dimension. The ballooning space (k-space) eigenfunctions are solved semi-analytically, while solutions in the second dimension (λ-space) are obtained by the standard perturbation theory. The continuum damping rate is written as a summation of contributions from the resonance points, each term resembling the Fermi golden rule formula. This clearly shows the quasi-mode nature of the continuum damped TAE, and indicates that the continuum damping can be properly interpreted as a transition process, i.e. the decaying of the TAE mode into the continuum modes. Numerical results are obtained for

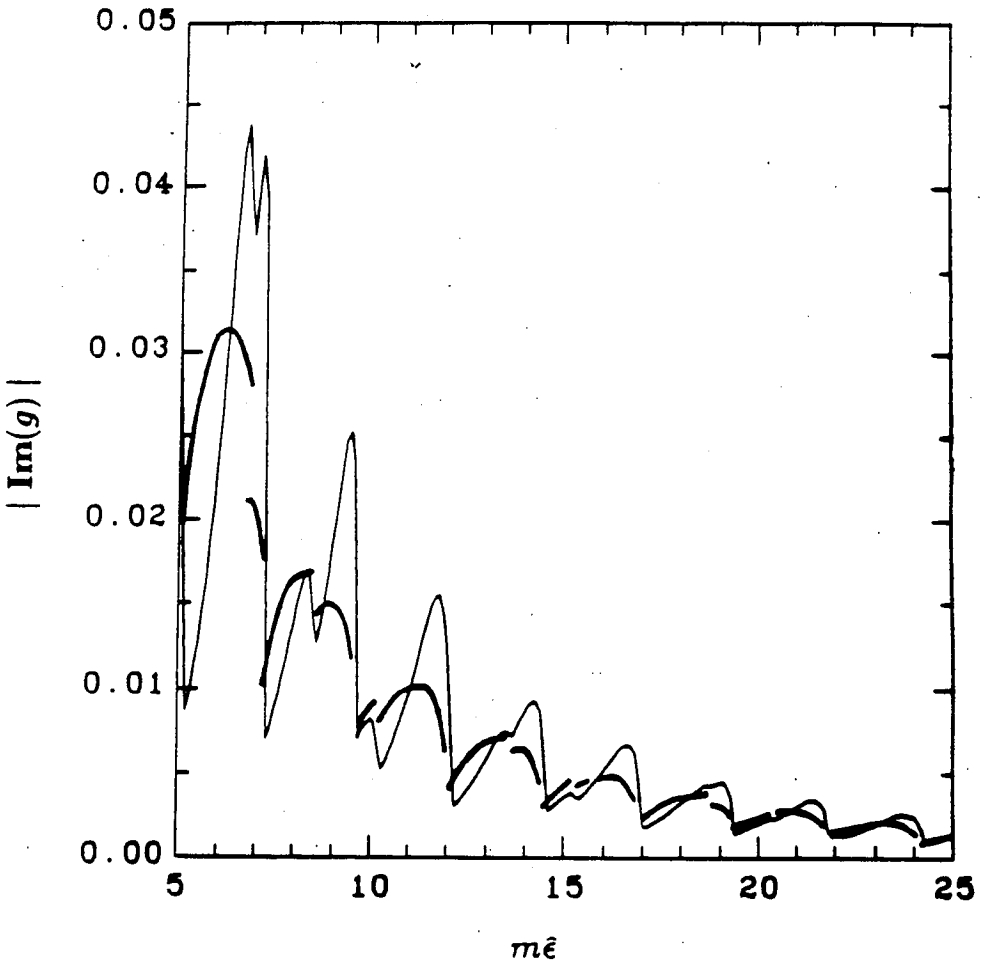

Figure 4.7: Comparison of the present calculation (thin line) with the results of Ref. [14] (thick line) for $s = 0.8$.

various shear parameters, and are in agreement with earlier calculations. The analysis also fills in the gaps left by earlier calculations; there are no intervals in the parameter $m\hat{\epsilon}$ where the roots could not be found. The damping rate is oscillatory and not a monotonic decreasing function of $m\hat{\epsilon}$. Although there is an overall decrease, the oscillatory behaviour is dominant, especially for strong shear and moderate mode numbers.

Chapter 5

Multiple-gap Theory of Toroidal Alfvén Waves with Kinetic Effects

5.1 Introduction

Kinetic effects on the toroidal Alfvén waves are studied in this chapter. It was first shown by Mett and Mahajan that the interaction of electron parallel dynamics with toroidicity could cause significant damping to the TAE. The higher damping was believed to be caused by a coupling between the TAE and the kinetic Alfvén wave (KAW) [39, 55, 56], in which energy was carried away by the KAW from the gap region. The effect was thus called "radiation damping". In addition, a new branch of modes emerge, which are formed by the coupling between KAW's. These new modes, called kinetic toroidal Alfvén eigenmodes (KTAE), have frequencies just above the shear Alfvén gap, and smoothly go over to the well-known kinetic Alfvén eigenmode in the slab limit. The KTAE closest to the gap was found to have a mode structure very similar to the TAE.

The kinetic effects on the stability of both the KTAE and the TAE (with a well-defined ideal limit) have been carried out in Ref. [29], where the theoretical framework is built around a single gap. This assumption seems to be plausible for very low toroidal mode number (n) and small magnetic shear, for which the adjacent gaps are well separated and the tunneling would be insufficient to induce a strong coupling between the gaps. However, for either

moderate n number and/or moderate magnetic shear, the coupling of gaps could be quantitatively significant. It is the purpose of this chapter to evaluate the multiple-gap effects on these two fundamental branches, the KTAE and the TAE.

A multiple-gap calculation is fundamentally a two-dimensional calculation, and must invoke an intrinsic toroidal coupling scheme. As we did in the last chapter, the formulation outlined in Chapter 2 is used. Again, linear profile is assumed for the local Alfvén frequency. It was shown in the last chapter that the convergence for a linear profile depends on the smallness of the inverse aspect ratio. As a result, the mode structure, although broad in the radial direction, does not show the conventional ballooning features. The envelop function $C(\lambda)$, instead of being localized near $\lambda = 0$ or π, oscillates with λ. And the global eigenvalue is an average of the parametrized ballooning eigenvalue over one period of the phase shift parameter λ, instead of being the extremum value at $\lambda = 0$ or π.

The necessary details of the formalism are given in Sec. (5.2), while in Sec. (5.3) numerical results are presented for the two fundamental branches. Comparison with single-gap results will be discussed in Sec. (5.4), where we also show how the basic equations for the single gap theory of Ref. [29] can be obtained from the ballooning formalism. A brief summary is given in Sec. (5.5).

5.2 Ballooning Theory for Toroidal Alfvén Waves with Kinetic Effects

The 2-D eigenmode equation describing shear Alfvén waves in a large aspect ratio axisymmetric tokamak with circular cross-section is modelled by

$$\frac{d}{dx}\left(\frac{\Omega^2 f(x)}{4}-(x-l)^2\right)\frac{d\phi_l}{dx}-\frac{1}{s^2}\left(\frac{\Omega^2 f(x)}{4}-(x-l)^2\right)\phi_l$$
$$+\epsilon\frac{\Omega^2}{4}\left(\frac{d^2\phi_{l+1}}{dx^2}+\frac{d^2\phi_{l-1}}{dx^2}\right)+\widehat{b}\left(\frac{d^2}{dx^2}-\frac{1}{s^2}\right)^2\phi_l=0, \qquad (5.1)$$

where, with the exception of the last term, everything is the same as in the equation for the ideal shear Alfvén waves in last chapter. In the last term, $\widehat{b}$ stands for the nonmagnetohydrodynamic effects (primarily the electron parallel response) measured by $(\rho_s k_\theta s)^2/4$ plus an imaginary part representing the electron Landau damping, and $k_\theta \equiv m/r$ is the poloidal wave number.

The physical meaning of individual terms in Eq. (5.1) is transparent: the first two constitute magnetic bending and ion inertia; and the remaining represent the toroidal coupling, and the electron kinetics, respectively. Neglecting $\hat{b}$ in Eq. (5.1) yields the equation for ideal toroidal shear Alfvén waves discussed in the last chapter. For $\epsilon = 0$, Eq. (5.1) reduces to the equation for kinetic shear Alfvén waves in slab geometry [39, 55, 56]. Although the coefficients of the last two terms of Eq. (5.1) are small, these two terms should not be treated as mere perturbations because they may (and, indeed do) create new branches of eigenmodes. For example, the toroidal coupling creates gaps in the shear Alfvén continuum and generates discrete modes in the gaps (the TAEs), while the kinetic term resolves the singularity in the equation and discretizes the shear Alfvén continuum.

Let the local Alfvén frequency be again approximated by a linear profile, i.e. $\Omega^2 f(x) \equiv 1 + \epsilon g(x)$ with $g(x) \approx g + 2x/m\widehat{\epsilon}$, where g is the order unity eigenvalue measuring the frequency shift from the center of the gap. Making use of the 2-D ballooning transform

$$\phi_l(x) = \oint d\lambda dk \exp[ik(x-l) - i\lambda l]\widehat{\Psi}(k,\lambda), \tag{5.2}$$

we obtain a 2-D equation in the k-λ representation

$$\left[\frac{\partial^2}{\partial k^2} + \frac{1+\epsilon g}{4} + \frac{\epsilon}{2}\cos(k+\lambda) - \frac{s^2}{(1+s^2k^2)^2} + b(1+s^2k^2) - \frac{i\epsilon}{2m\widehat{\epsilon}}\frac{\partial}{\partial\lambda}\right]\Psi(k,\lambda) = 0, \tag{5.3}$$

with $b \equiv \widehat{b}/s^2$, for the scaled variable $\Psi \equiv \widehat{\Psi}\sqrt{1+s^2k^2}$. The zeroth order ballooning equation is

$$\mathcal{L}[\lambda]\chi(k,\lambda) = 0, \tag{5.4}$$

with

$$\mathcal{L}[\lambda] \equiv \frac{\partial^2}{\partial k^2} + \frac{1+\epsilon\tilde{g}(\lambda)}{4} + \frac{\epsilon}{2}\cos(k+\lambda) - \frac{s^2}{(1+s^2k^2)^2} + b(1+s^2k^2), \tag{5.5}$$

where $\chi(k,\lambda)$ is the eigenfunction, while $\tilde{g}(\lambda)$ is the parametrized (λ-dependent) eigenvalue of $\mathcal{L}[\lambda]$.

Note that the operator $\mathcal{L}$ is no longer self-adjoint, since the parameter b is complex. Nonetheless the following equation holds for arbitrary functions $\chi_1(k,\lambda)$ and $\chi_2(k,\lambda)$:

$$\int dk \chi_1 \mathcal{L}[\lambda]\chi_2 = \int dk \chi_2 \mathcal{L}[\lambda]\chi_1. \tag{5.6}$$

The annihilation process in Chapter 2 is therefore more conveniently done by multiplying with χ_p (instead of χ_p^*) and integrating. Neglecting cross coupling terms in Eq. (2.53), we get

$$\frac{2i}{m\widehat{\epsilon}}\frac{dC(\lambda)}{d\lambda} - [g - \widehat{g}(\lambda)]C(\lambda) = 0, \tag{5.7}$$

for the function $C(\lambda)$, where the spectrum index is dropped, and

$$\widehat{g}(\lambda) = \widetilde{g}(\lambda) + \frac{2i}{m\widehat{\epsilon}}\langle\chi \mid \frac{\partial\chi}{\partial\lambda}\rangle. \tag{5.8}$$

Here the bracket operator is defined as

$$\langle\chi_1(k,\lambda) \mid \chi_2(k,\lambda)\rangle \equiv \int dk\chi_1(k,\lambda)\chi_2(k,\lambda). \tag{5.9}$$

Solving Eq. (5.7) with the requirement that $C(\lambda)$ be periodic in λ yields

$$g = \oint d\lambda\widehat{g}(\lambda) - \frac{2N}{m\widehat{\epsilon}}, \tag{5.10}$$

and

$$C(\lambda) = \exp\left(-\frac{im\widehat{\epsilon}}{2}\int_0^\lambda d\lambda'\,[g - \widehat{g}(\lambda')]\right), \tag{5.11}$$

where N in an integer. These equations are the same as the zeroth order solution in the last chapter, but here damping enters through the parametrized eigenvalue $\widetilde{g}(\lambda)$.

5.3 2-D Eigenvalues and Mode Structure

In the ideal limit, the ballooning equation (Eq. (5.4)) reduces to Eq. (4.16), studied in last chapter. The dispersion relation for the TAE in the first gap can be put in the form

$$\Delta_1\widetilde{g}(\lambda) + \Delta_2\sqrt{1 - \widetilde{g}^2(\lambda)} = \cos\lambda, \tag{5.12}$$

where Δ_1 and Δ_2 can be obtained from the phase shifts δ_1 and δ_2 tabulated in Chapter 4. Numerical values for Δ_1 and Δ_2 can also be found in Ref. [14]. For weak shear, both Δ_1 and Δ_2 are large, so that $\tilde{g}(\lambda)$ tends to be λ-independent. On the other hand, as the magnetic shear becomes large, Δ_2 goes to zero very rapidly. As a result, $\tilde{g}(\lambda)$ is well approximated by $\cos\lambda$, and the 2-D eigenvalue g goes to zero upon averaging over λ.

In the general case, Eq. (5.12) can be solved for $\tilde{g}(\lambda)$, and when substituted into Eq. (5.10), yields the 2-D eigenvalue

$$g = -\frac{2\Delta_2}{\pi}\sqrt{\Delta_1^2+\Delta_2^2}\,E\left(\frac{1}{\Delta_1^2+\Delta_2^2}\right), \tag{5.13}$$

where we have chosen $N = 0$, and neglected the self-coupling term since it only introduces a correction of order $\mathcal{O}(1/m\hat{\epsilon})$. The function E here is the complete elliptic integral of the second kind, defined by

$$E(\kappa^2) = \int_0^{\pi/2} d\phi\sqrt{1-\kappa^2\sin^2\phi}. \tag{5.14}$$

With the electron kinetics, the 2-D eigenvalues are obtained by numerical methods. We first solve [using a shooting code] the ballooning equation [Eq. (5.4)] to obtain the parametrized eigenvalue $\tilde{g}(\lambda)$. The numerically obtained $\tilde{g}(\lambda)$ is then averaged over λ to yield the kinetic eigenvalue g, which now contains damping.

The eigenfunctions for TAE and KTAE are plotted in Figs. 5.1 and 5.2, respectively, for $s = 0.5, \epsilon = 0.2, |b| = 6\times10^{-5}$, and $\mathrm{Arg}b = -0.2$. It can be seen that the TAE and the KTAE have similar structures, but a different parities. For $\lambda = 0$, the TAE has even parity, while the KTAE has odd parity. For $\lambda = \pi$, it's just the opposite. Another character is that the TAE structure

(in particular, the mode extension) is more sensitive to the parameter λ. The same is true for the parametrized TAE eigenvalue. This character stems from the fact that the TAE is a genuine 2-D mode, which in turn implies that the TAE has a more extended radial structure and multiple-gap coupling may be more important.

For the TAE branch, the λ dependence of the real (imaginary) part of $\tilde{g}(\lambda)$ is displayed in Fig. 5.3a [Fig. 5.3b] for various values of the shear parameter $s = 0.2, 0.5$, and 1.0, with $\epsilon = 0.2$. The complex parameter b is represented by its absolute value $|b|$ and the phase Arg $b \equiv \tan^{-1}(\mathrm{Im}b/\mathrm{Re}b)$, for which we use $|b| = 6 \times 10^{-5}$ and Arg b = -0.2. The λ-dependence of $\tilde{g}$ is qualitatively similar to that described by the analytic dispersion, Eq. (5.12) for the ideal mode, i.e., it is very weak at small shear, and tends to be oscillatory around zero for large shear. The large damping rate for $\lambda = \pi$ in the present ballooning calculation would make the average damping rate to be quite different from the lowest ($\lambda = 0$) damping rate predicted by the conventional ballooning approach. This intrinsic 2-D effect will have important consequences for the stability of TAE.

For the KTAE branch, the λ dependence of the real (imaginary) part of $\tilde{g}(\lambda)$ is displayed in Fig. 5.4a [Fig. 5.4b] for various values of the shear parameter. Again, the λ-dependence of $\tilde{g}$ is stronger for larger shear. However, comparing with the TAE, this λ-dependence is much weaker, and $\mathrm{Re}(\tilde{g})$ is never near zero. These two features suggest the one-dimensional origin of the mode, and indicate that the effects of multiple-gap coupling on the KTAE are expected to be weak.

The results of Figs. 5.3 and 5.4 also indicate that $\mathrm{Re}(\tilde{g})$ is much greater than $\mathrm{Im}(\tilde{g})$. As a result, $C(\lambda)$ is essentially a purely oscillatory function of λ,

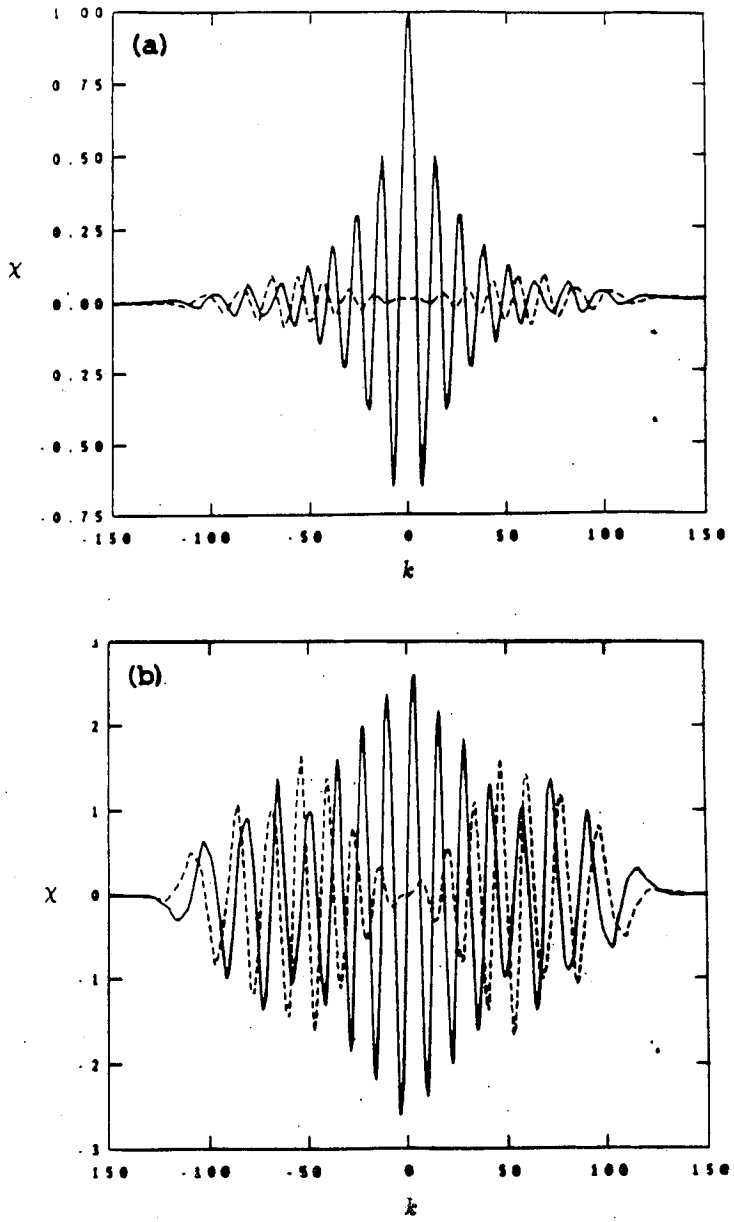

Figure 5.1: The TAE mode structure for $s = 0.5, \epsilon = 0.2, |b| = 6 \times 10^{-5}$, and $\mathrm{Arg}b = -0.2$. Part (a) is for $\lambda = 0$ and part (b) for $\lambda = \pi$. Solid line represents the real part of the eigenfunction, and broken line represents the imaginary part.

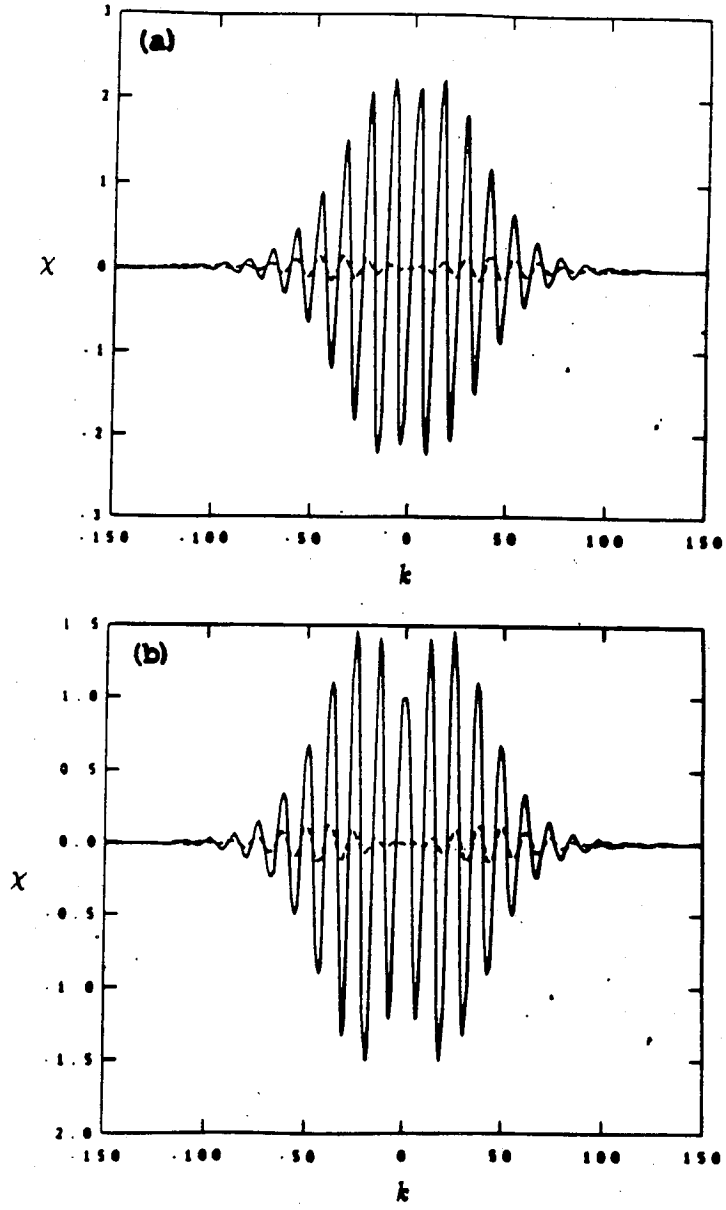

Figure 5.2: The KTAE mode structure for $s = 0.5, \epsilon = 0.2, |b| = 6 \times 10^{-5}$, and $\mathrm{Arg}b = -0.2$. Part (a) is for $\lambda = 0$ and part (b) for $\lambda = \pi$. Solid line represents the real part of the eigenfunction, and broken line represents the imaginary part.

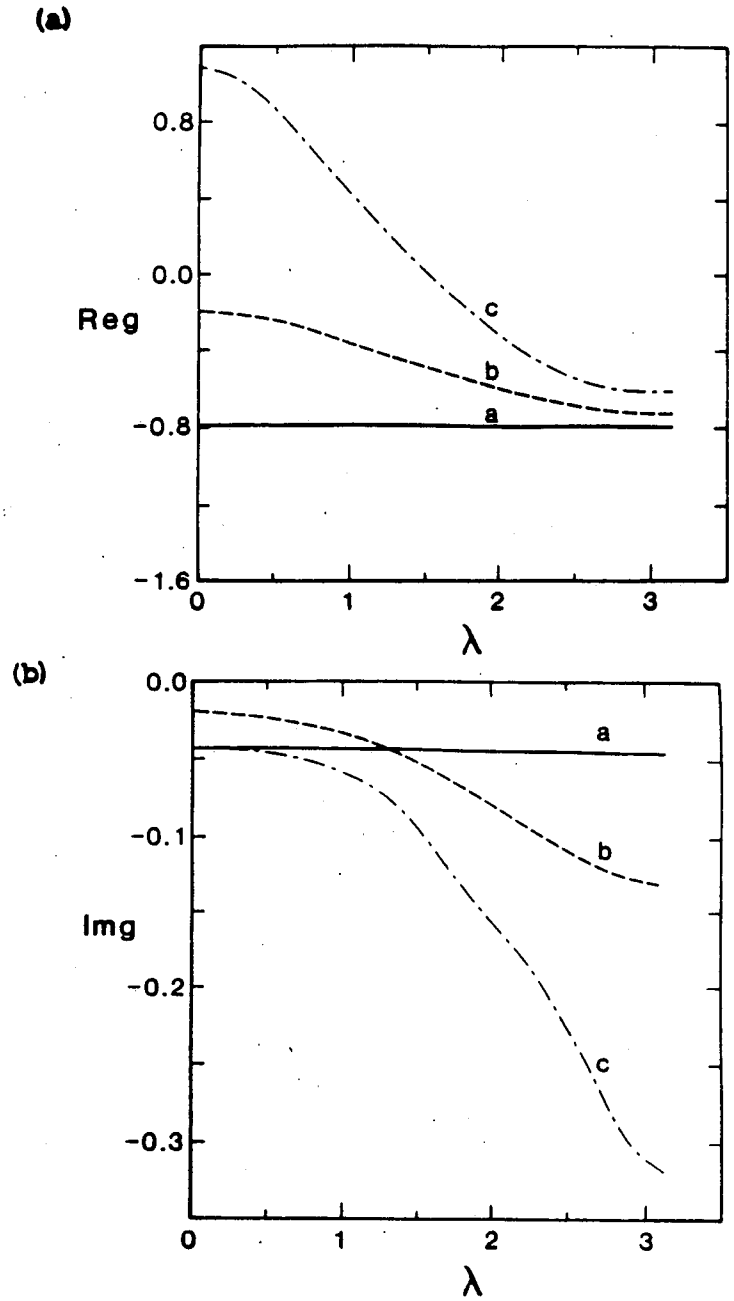

Figure 5.3: The parameterized eigenvalues of the TAE as a function of λ. The real part is plotted in (a), imaginary part is plotted in (b). The curves a, b, and c, stand for $s = 0.2, 0.5$, and 1.0, respectively, with $|b| = 6 \times 10^{-5}$, Arg$b = -0.2$, and $\epsilon = 0.2$.

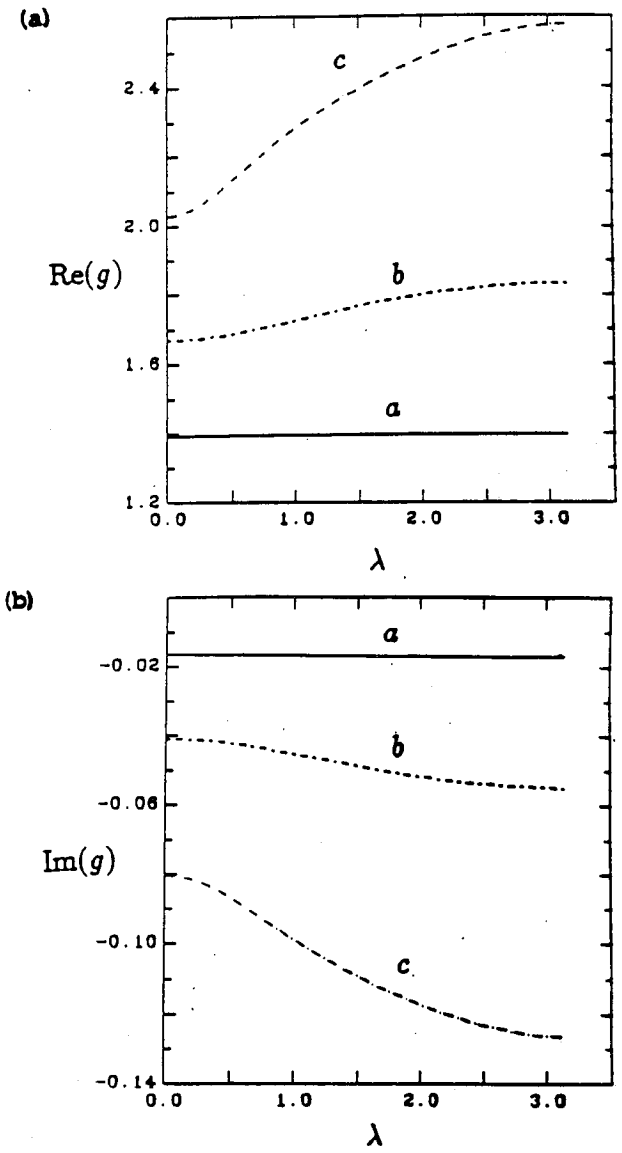

Figure 5.4: The parameterized eigenvalues of the KTAE as a function of λ. The real part is plotted in (a), imaginary part is plotted in (b). The curves a, b, and c, stand for $s = 0.2, 0.5$, and 1.0, respectively, with $|b| = 6 \times 10^{-5}$, Arg$b = -0.2$, and $\epsilon = 0.2$.

as in the ideal case studied in the last chapter. Thus the mode structure is quite different from that in the conventional ballooning picture, in particular, it has no ballooning feature in the poloidal direction. The radial extension of this non-ballooned mode is measured by $\Delta r \sim \epsilon r$ with a suppression factor arising from the weak λ-dependence of $\tilde{g}$ either for the small magnetic shear or for the KTAE branch.

The 2-D eigenvalues for TAE (KTAE) are plotted in Figs. 5.5a, 5.5b (Figs. 5.6a, 5.6b) as functions of the parameter $|b|s^2$, which measures the strength of the kinetic term. For all these cases $\epsilon = 0.2$, and the shear values of 0.2, 0.5, and 1.0 are labelled by the letters a, b and c respectively. In addttion, the curves with subscript 2 are obtained from the present theory which naturally includes the multiple-gap coupling, whereas the curves with subscript 1 are obtained from the single gap theory for comparison. In Sec. (5.4), we will show that the single-gap theory of Ref. [29] is a limiting case of the present theory. Large shear pushes Re(g) of the TAE towards zero, i.e., towards the center of the gap. However, the shear effect on the real eigenvalues of the KTAE, which resides in the continuum, is not as strong as it is for the TAE.

The magnetic shear augments damping rates for both TAE and KTAE, and stronger for KTAE. However, the TAE suffers stronger damping than KTAE in regions of parameters where kinetic effects are moderately strong; i.e., for high temperature, moderate shear and moderate mode numbers. It may be thus easier to excite KTAE than TAE in the interesting parameter regimes. This tendency is demonstrated in Fig. 5.7, where we find that as $|b|$ increases, there is a critical value (dependent on s) beyond which KTAE is less damped than TAE.

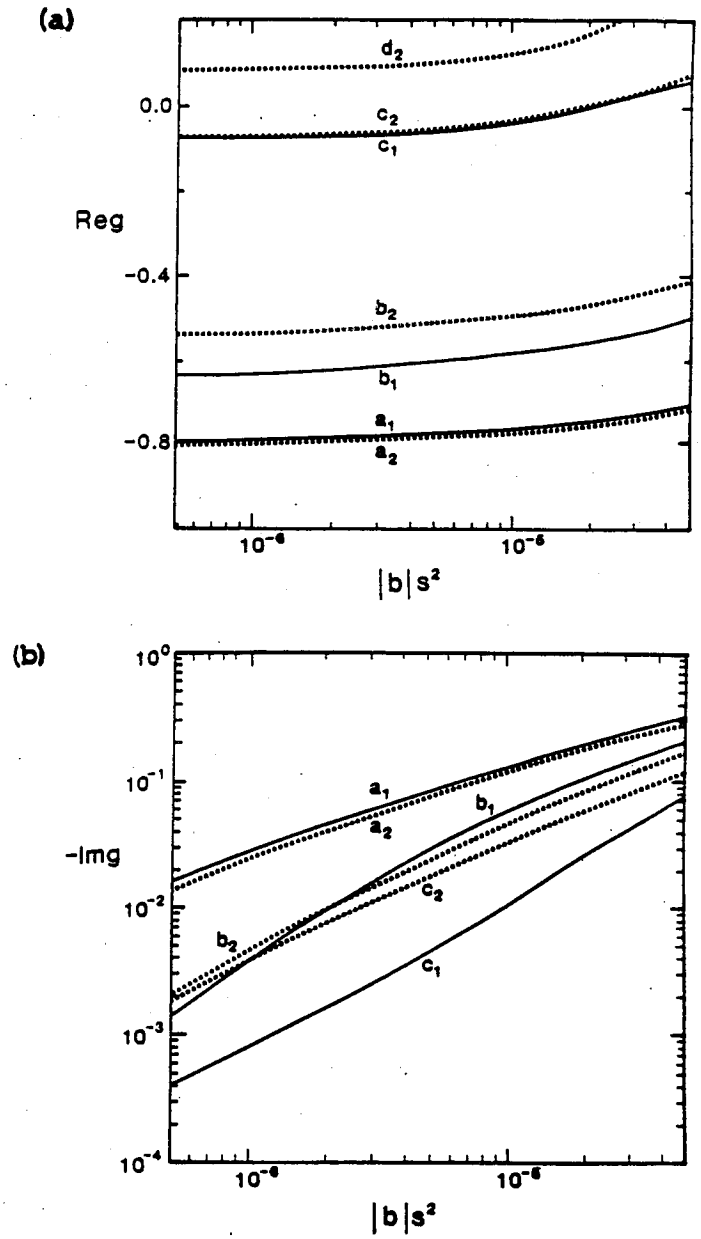

Figure 5.5: The 2-D eigenvalue of the TAE vs. $|b|s^2$ with $\epsilon = 0.2$. The real part is plotted in (a) and the imaginary part is plotted in (b). The subscripts 1 and 2 represent the results from the single gap the multiple-gap theory, respectively. The curves a, b, c, and d stand for shear parameters $s = 0.2, 0.5, 1.0$, and 2.0.

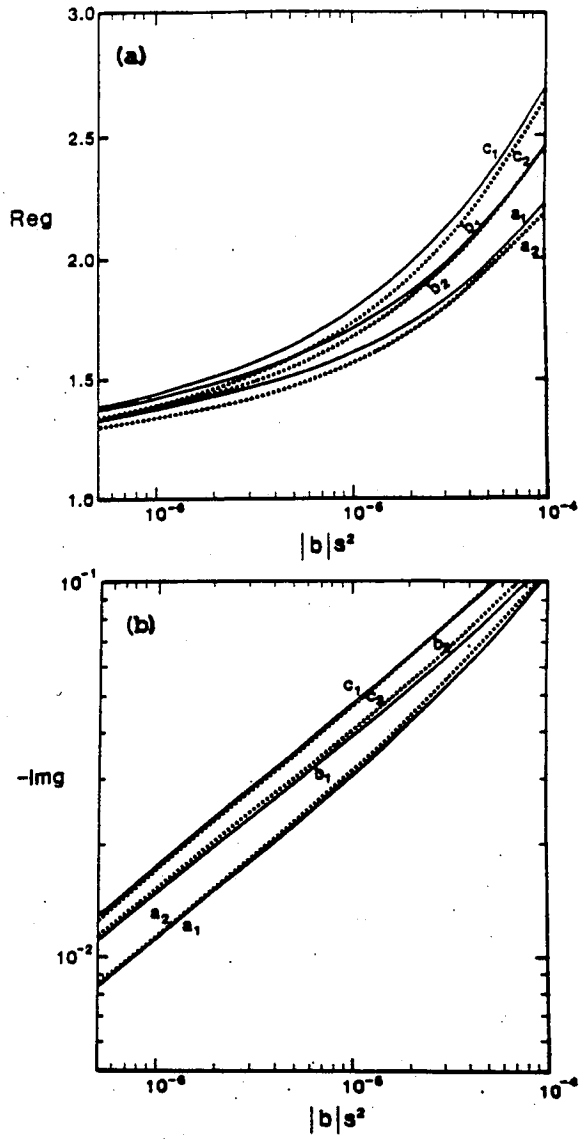

Figure 5.6: The 2-D eigenvalue of the KTAE vs. $|b|s^2$ with $\epsilon = 0.2$. The real part is plotted in (a) while the imaginary part is plotted in (b). The subscripts 1 and 2 represent the results from the single gap the multiple-gap theory, respectively. The curves a, b, and c stand for shear parameters $s = 0.2, 0.5$, and 1.0.

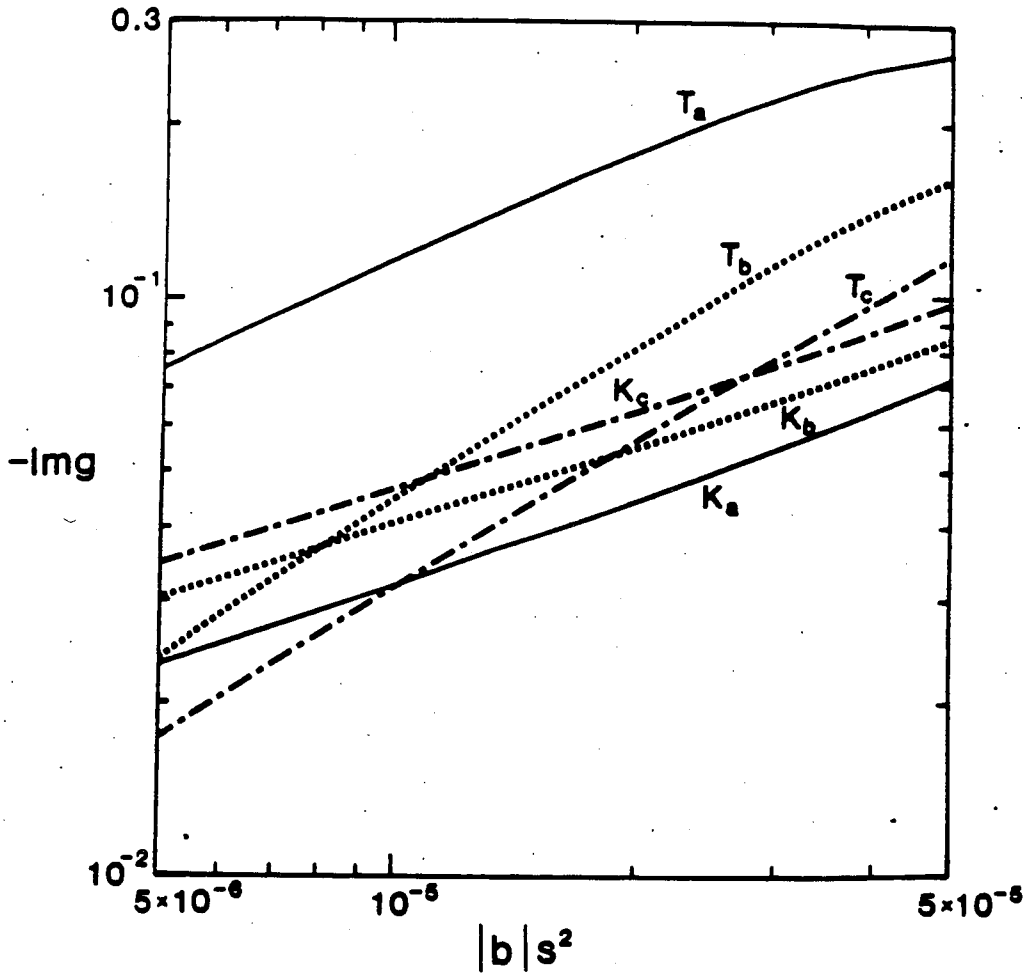

Figure 5.7: Comparison of the damping rate for TAE (curves T_a – T_c) and KTAE (curves K_a – K_c) for $\epsilon = 0.2$. The subscripts a, b, and c stand for $s = 0.2, 0.5$, and 1.0, respectively.

The strong kinetic damping on TAE is also related to the kinetic effects on the mode structure. The ideal TAE mode extension in k-space, primarily measured by $k \sim 4/\epsilon\sqrt{1-\tilde{g}^2}$, could be greatly modified by the electron kinetics that tends to capture the mode in a much less extended k region. This mechanism for the enhancement of damping rate due to electron kinetics requires an intrinsic inclusion of the kinetics; a simple-minded perturbative estimate presuming ideal mode structure will not do. These conclusions are supportive, and are in essential qualitative agreement with the basic results of the single gap theory of Ref. [29]

5.4 Transit to Single-Gap Theory

In the small shear limit, the ballooning equation (Eq. (5.4)) can be converted to a solvable system by taking averages over the fast scale arising from toroidicity. Writing χ as

$$\chi(k,\lambda) = \chi_+ e^{-ik/2} + \chi_- e^{ik/2}, \tag{5.15}$$

and averaging over k weighted with $e^{ik/2}$ and $e^{-ik/2}$, one obtains a set of coupled equations for χ_+ and χ_- (c.f. Ref. [9], also Chapter 4). These two equations are

$$\left[\frac{d^2}{dk^2} + i\frac{d}{dk} + h(k)\right]\chi_- = -\frac{\epsilon}{4}\exp(i\lambda)\chi_+, \tag{5.16}$$

$$\left[\frac{d^2}{dk^2} - i\frac{d}{dk} + h(k)\right]\chi_+ = -\frac{\epsilon}{4}\exp(-i\lambda)\chi_-, \tag{5.17}$$

where

$$h(k) = \frac{\epsilon g}{4} - F(k) - b(1+s^2k^2), \tag{5.18}$$

with $F(k) \equiv s^2/(1+s^2k^2)^2$.

The explicit λ dependence has no effect on the eigenvalue determined by Eqs. (5.16) and (5.17), because $\exp(\pm i\lambda)$ can be absorbed into the wave amplitudes $\chi_\pm$. For example, one can introduce $\widehat{\chi}_+ = \chi_+ \exp(i\lambda)$, so that both $\widehat{\chi}_+$ and χ_- are λ-independent. This λ-independence of the averaged equations is not surprising, for λ is just a phase shift, which is effectively averaged along with the average over the fast scale. For the averaged equations, the scale lengths for $\chi_\pm$ are much greater than unity due to their slow variations, so that the second derivatives can be neglected. Then, the coupled equations (5.16) and (5.17) are reduced to two first order differential equations, the basic equations derived under the single-gap assumption, except that in h the G-term of Ref. [29] is replaced by the F-term. As $s\bar{k} \gg 1$ (where $\bar{k}$ is the length scale of $\chi_\pm$, for small but finite b, $s\bar{k} \sim (s/b)^{1/3} \gg 1$), there exists only two independent parameters (the coefficients of the F-term and the kinetic term) that may enter into the dispersion. For the KTAE branch, since the F-term is not crucial, only one independent parameter $(4s\rho_s k_\theta/\epsilon)^2$ ($\equiv \widehat{\tau}/\widehat{\epsilon}^3$ of Ref. [29]) may come into the dispersion. This is just the KTAE scaling of Ref. [29].

It is worth noting that the small shear limit implies a weak λ-dependence for the parametrized eigenvalue $\widetilde{g}(\lambda)$ of the ballooning equation. For the averaged equations, the eigenvalue $\widetilde{g}(\lambda)$ is independent of λ. The lowest ($N = 0$) mode for Eq. (5.11) is then given by $C(\lambda) =$ constant. And the entire wavefunction in k-λ space is

$$\widehat{\Psi}(k,\lambda) = \frac{1}{\sqrt{1+s^2k^2}} \left(\widehat{\chi}_+(k) e^{-i\lambda - ik/2} + \chi_-(k) e^{ik/2} \right) \tag{5.19}$$

where we have brought back the scale factor $\sqrt{1+s^2k^2}$. Substituting Eq. (5.19)

back into the 2-D ballooning transform (Eq. (5.2)), we get

$$\phi(x,\theta) \equiv \sum_l \phi_l(x) e^{-il\theta}$$

$$= \int dk \frac{\widehat{\chi}_+(k)}{\sqrt{1+s^2k^2}} e^{ik(x+1/2)} e^{i\theta} + \int dk \frac{\chi_-(k)}{\sqrt{1+s^2k^2}} e^{ik(x+1/2)}. \quad (5.20)$$

It can be seen that the mode consists of two poloidal harmonics, one with $l=-1$, the other with $l=0$, both are centered at the position $x=-1/2$. This is exactly the single gap mode structure.

We note that it is equally legitimate to absorb the λ dependent exponential factor into χ_- and define $\widehat{\chi}_- = \chi_- \exp(-i\lambda)$. One would then get a set of equations for $\widehat{\chi}_-$ and χ_+ which are exactly the same as for χ_- and $\widehat{\chi}_+$. When this new set of solutions are substituted into the 2-D ballooning transform, it yields a mode centered at $x=1/2$, consisting of the poloidal harmonics $l=0$ and $l=1$, which is the solution for neighbouring gaps. It seems that the eigenvalues for these two solutions would be the same, violating the assumption of linear profile for the local Alfvén frequency. This apparent inconsistency is resolved by including the self-coupling term in the eigenvalue. For the former mode located at $x=-1/2$, the correction is

$$\Delta_g^1 = \frac{2i}{m\widehat{\epsilon}} \frac{\langle \chi \mid \partial\chi/\partial\lambda \rangle}{\langle \chi \mid \chi \rangle}$$

$$= \frac{1}{m\widehat{\epsilon}}, \quad (5.21)$$

and for the latter (located at $x=1/2$), the correction is $\Delta_g^2 = -1/(m\widehat{\epsilon})$, in complete agreement with the quantization rule Eq. (5.10) and the linear profile assumption.

Physically, weak shear implies that the separation between the gaps is large and the wavefunction localized in these gaps do not overlap. For this reason the eigenvalue becomes independent of λ in the weak shear limit, and multiple-gap coupling tends to diminish. Quantitative comparison of the theory with multiple-gap coupling, to the single gap theory is also presented in Figs. 5.5a, 5.5b (Figs. 5.6a, 5.6b) for TAE (KTAE). Numerical results for the single gap theory are obtained by solving Eqs. (5.16) and (5.17) with the second derivative terms (d^2/dk^2) neglected. For magnetic shear near 1.0 the theory with multiple-gap coupling predicts a stronger damping rate then that given by the single gap theory (by a factor of $\simeq 2$) for the TAE branch. However, the effect from multiple-gap coupling is not significant for the KTAE branch. The discrepancy between the two theories is noticeable for large shear and tends to become negligible as the magnetic shear becomes small.

5.5 Summary

The primary purpose of this chapter is to calculate the effects of multiple-gap coupling on the mode damping rates, in particular, the damping induced by parallel electron dynamics. For this purpose, the 2-D ballooning approach outlined in Chapter 2 is used. Multiple-gap coupling enters through the λ-dependence of the parametrized eigenvalue $\tilde{g}(\lambda)$ of the ballooning equation. A linear profile for the local Alfvén frequency is assumed, for which, convergence of the theory depends on the smallness of the inverse aspect ratio. The 2-D eigenvalue g is an average of the parametrized ballooning eigenvalue $\tilde{g}(\lambda)$ over a period of λ. As a consequence, the damping rate is higher than the minimum damping predicted by the extremum value of $\tilde{g}(\lambda)$ at $\lambda = 0$ or π,

as one would get from conventional ballooning theory. The eigenfunction also differs from that of conventional ballooning theory, it does not show the usual ballooning features, and its radial extension is measured by $\Delta r \sim \epsilon r$ instead of the usual $r/\sqrt{n}$.

Comparison is made with the single gap theory of Ref. [29]. It is found that the multiple-gap coupling is more significant for the TAE than for the KTAE. As an example, for $s \sim 1.0$ the multiple-gap theory predicts a stronger damping rate for the TAE than given by the single-gap theory (by a factor $\simeq 2$). In the small shear limit, however, the multiple-gap theory smoothly reduces to the single-gap theory.

Chapter 6

Summary

In this thesis, we present a general formalism for high n (n is the toroidal mode number) modes in an axisymmetric toroidal plasma, with applications to the toroidal Alfvén eigenmodes. The formulation is based on the two dimensional (2-D) ballooning transformation [10].

In Chapter 2, We gave a general description of the ballooning approach with a review of the conventional theory, and a formal development of the 2-D approach. A specific example for the 2-D formulation is given in Chapter 3, where we solved the model equations [of Ref. [16]] for the toroidal drift waves and for the resistive interchange modes in a toroidal pinch. Comparison is made with the conventional theory of Connor, Hastie and Taylor [2]; we have shown that our 2-D formulation is more general than the conventional theory, and it reduces to the conventional theory in a special case. The relationship between the conventional ballooning feature and "another" type of ballooning [16] is also discussed.

In Chapter 4, we studied the continuum damping of the ideal toroidal Alfvén eigenmodes (TAE). A perturbation theory based on the 2-D ballooning formulation is systematically developed. The continuum damping rate is expressed explicitly in terms of the coupling of the TAE to the continuum spectrum. It is shown that the continuum damping can be properly interpreted as a transition process, i.e. the decaying of the TAE mode into continuum modes.

Numerical results are obtained for various plasma parameters and compared with previous calcultaions. It is found that the damping rates are oscillatory with the parameter $m\hat{\epsilon}$ (which signifies the spacial variation of the local Alfvén speed), and in some narrow intervals of $m\hat{\epsilon}$ the damping rates vary very rapidly. These regions correspond precisely to the root missing intervals of the numerical solution by Rosenbluth *et al.* [14].

Kinetic effects on the toroidal Alfvén waves are studied in Chapter 5. Multiple-gap coupling is automatically taken care of by the 2-D ballooning formulation. In the kinetic theory, a new branch of the mode emerges. Aptly named the kinetic toroidal Alfvén eigenmode (KTAE), it resides just above the toroidal Alfven gap, and has a structure very similar to the TAE. Numerical results are obtained and compared to the single gap theory by Mett and Mahajan [29]. Multiple-gap coupling effects are found to be more significant for moderate to large magnetic shear and for the TAE (as compared with the KTAE). In some parameter regimes, the KTAE is less damped than the TAE. When the magnetic shear s becomes small, the ballooning theory with multiple-gap coupling smoothly reduces to the single gap theory.

Appendix A

Coupling Matrix Elements for Continuum Damping of TAE

From the orthogonality properties, we have

$$\langle \chi_0 \mid \mathcal{L}[\lambda] \mid \psi_{\tilde{g}}^{(\pm)} \rangle = -\frac{1+\epsilon\tilde{g}}{4} \langle \chi_0 \mid \psi_{\tilde{g}}^{(\pm)} \rangle = 0. \tag{A.1}$$

Differentiating Eq. (A.1) with respect to λ, we obtain

$$\left\langle \chi_0 \mid \frac{\partial \psi_{\tilde{g}}^{(\pm)}}{\partial \lambda} \right\rangle = \frac{2}{\tilde{g} - g_0(\lambda)} \langle \chi_0 \mid \sin(k+\lambda) \mid \psi_{\tilde{g}}^{(\pm)} \rangle. \tag{A.2}$$

Straightforward algebra yields

$$\left\langle \chi_0 \mid \frac{\partial \psi_{\tilde{g}}^{(\pm)}}{\partial \lambda} \right\rangle = \frac{4i}{\epsilon(\tilde{g} - g_0)} \frac{2\beta}{N_c N_0 (\tilde{g}^2 - g_0^2)} \times$$

$$\left\{ (\tau_r \tau_R + 1) e^{i\Theta/2} \mathrm{Re} \left[e^{i(\Theta - \Theta_+)/2} \left(1 - B_+ + \frac{2i\beta_0}{\beta - \tilde{g} - Y_+} \right) \right] \right.$$

$$\left. \pm i(\tau_r - \tau_R) e^{i\Theta/2} \mathrm{Re} \left[e^{i(\Theta - \Theta_-)/2} \left(1 - B_- + \frac{2i\beta_0}{\beta - \tilde{g} - Y_-} \right) \right] \right\}.$$

BIBLIOGRAPHY

[1] J.W. Connor, R.J. Hastie, and J.B. Taylor, Phys. Rev. Lett. **40**, 396 (1978).

[2] J.W. Connor, R.J. Hastie, and J.B. Taylor, Proc. R. Soc. Lond. A. **365**, 1 (1979).

[3] Y.C. Lee and J.W. Van Dam, in *Proceedings of the Finite Beta Theory Workshop*, Varenna Summer School of Plasma Physics, September 1977, Varenna, Italy, edited by B. Coppi and B. Sadowski (U.S. Department of Energy, Office of Fusion Energy, Washington D.C., 1979), CONF-7709167, p. 93.

[4] A. Glasser, in Ref. 3, p. 55.

[5] R.J. Hastie, K.W. Hesketh, J.B. Taylor, Nuclear Fusion **19**, 1223 (1979).

[6] Liu Chen and C.Z. Cheng, Phys. Fluids, **23**, 2242 (1980).

[7] F. Romanelli, Phys. Fluids B **1**, 1018 (1989).

[8] J.Q. Dong, W. Horton, and J.Y. Kim, Phys. Fluids B **4**, 1867 (1992).

[9] C.Z. Cheng, L. Chen, and M.S. Chance, Ann. Phys. (NY) **161**, 21 (1985).

[10] Y.Z. Zhang and S.M. Mahajan, Phys. Lett. A **157**, 133 (1991).

[11] F. Pegoraro, T.J. Schep, Phys. Fluids **24**, 478 (1981).

[12] J.W. Connor, J.B. Taylor, and H.R. Wilson, Phys. Rev. Lett. **70**, 1803 (1993).

[13] Y.Z. Zhang, S.M. Mahajan, and X.D. Zhang, Phys. Fluids B **4**, 2729 (1992).

[14] M.N. Rosenbluth, H.L. Berk, J.W. Van Dam, and D.M. Lindberg, Phys. Rev. Lett. **68**, 596 (1992).

[15] F. Zonca and L. Chen, Phys. Rev. Lett. **68**, 592 (1992).

[16] J.W. Connor and J.B. Taylor, Phys. Fluids **30**, 3180 (1987).

[17] E.M. Barston, Ann. Phys. **29**, 282 (1964).

[18] Z. Sedlacek, J. Plasma Phys. **5**, 239 (1971).

[19] C. Uberoi, Phys. Fluids **15**, 1673 (1972).

[20] C.Z. Cheng and M.S. Chance, Phys. Fluids **29**, 3695 (1986).

[21] D.J. Sigmar, C.T. Hsu, R. White, and C.Z. Cheng, Phys. Fluids B **4**, 1506 (1992).

[22] G.Y. Fu and J.W. Van Dam, Phys. Fluids B **1**, 1949 (1989).

[23] G.Y. Fu and C.Z. Cheng, Phys. Fluids B **2**, 985 (1990).

[24] K.L. Wong, R.J. Fonck, S.F. Paul, D.R. Roberts, E.D. Fredrickson, R. Nazikian, H.K. Park, M. Bell, N.L. Bretz, R. Budny, S. Cohen, G.W. Hammett, F.C. Jobes, D.M. Meade, S.S. Medley, D. Mueller, Y. Nagayama, D.K. Owens, and E.J. Synakowski, Phys. Rev. Lett. **66**, 1874 (1991).

[25] W.W. Heidbrink, E.J. Strait, E. Doyle, and R. Snider, Nucl. Fusion **31**, 1635 (1991).

[26] H.L. Berk, J.W. Van Dam, Z. Guo, and D.M. Lindberg, Phys. Fluids B **4**, 1806 (1992).

[27] R. Betti and J.P. Freidberg, Phys. Fluids B **4**, 1465 (1992).

[28] N.N. Gorelenkov and S.E. Sharapov, Phys. Scr. **45**, 163 (1992).

[29] R.R. Mett and S.M. Mahajan, Phys. Fluids B **4**, 2885 (1992).

[30] R.R. Mett and S.M. Mahajan, in *Theory of Fusion Plasmas, Proceedings of the joint Varenna-Lausanne International Workshop*, Varenna, 1992, edited by J. Vaclavik, F. Troyon, and E. Sindoni (Editorie Compositori Societa Italiana di Fisica, Bologna, 1993).

[31] M.S. Chu, A.D. Turnbull, J.M. Greene, L.L. Lao, M.S. Chance, H.L. Berk, B.N. Breizman, W.Q. Li, D.M. Lindberg, S.M. Mahajan, R.R. Mett, D.W. Ross, J.W. Van Dam, J.C. Wiley, H. Ye, J. Candy, and M.N. Rosenbluth, in *Proceedings of the 14th International Conference on Plasma Physics and Controlled Nuclear Fusion Research*, Wurzberg, Germany (International Atomic Energy Agency, Vienna, 1993), Vol. 1, p. 855.

[32] R.D. Hazeltine and J.D. Meiss, Phys. Reports **121**, 1 (1985).

[33] C. Mercier, Nucl. Fusion **1**, 47 (1960).

[34] R.D. Hazeltine, W.A. Newcomb, Phys. Fluids B **2** 7 (1990).

[35] J.W. Van Dam, Ph. D. Thesis, Univ. of California, Los Angeles, 1979.

[36] R.D. Hazeltine, R.J. Hitchcock, and S.M. Mahajan, Phys. Fluids **24**, 180 (1981).

[37] W.A. Newcomb, Phys. Fluids B **2**, 86 (1990).

[38] R.L. Dewar in *Theory of Fusion Plasmas, Proceedings of the Varenna Workshop on Theory of Fusion Plasmas*, Varenna, Italy, 1987, Eds. A. Bonderson, E. Sindoni and F. Troyon (Societa Italiana di Fisica, Bologna, 1988).

[39] D.W. Ross, G.L. Chen, and S.M. Mahajan, Phys. Fluids **25**, 652 (1982).

[40] K. Appert, R. Gruber, F. Troyon, and J. Vaclavik, Plasma Phys. **24**, 1147 (1982).

[41] S.M. Mahajan, D.W. Ross, and G.L. Chen, Phys. Fluids **26**, 2195 (1983).

[42] Y.M. Li, S.M. Mahajan, and D.W. Ross, Phys. Fluids **30**, 1466 (1987).

[43] G.Y. Fu and J.W. Van Dam, Phys. Fluids B **1**, 2404 (1989).

[44] S. Riyopoulos and S.M. Mahajan, Phys. Fluids **29**, 731 (1986).

[45] R.L. Dewar, R.C. Grimm, J.L. Johnson, E.A. Frieman, J.M. Greene, and P.H. Rutherford, Phys. Fluids **17**, 930 (1974).

[46] R. Betti and J.P. Freidberg, Phys. Fluids B **3**, 1865 (1991).

[47] M.S. Chu, J.M. Greene, W. Ling, A.D. Turnbull, H.L. Berk, and M.N. Rosenbluth, Phys. Plasmas **1**, 1214 (1994).

[48] H.L. Berk, R.R. Mett, and D.M. Lindberg, Phys. Fluids B **5**, 3969 (1993).

[49] Fulvio Zonca and Liu Chen, Phys. Fluids B **5**, 3668 (1993).

[50] Huanchun Ye, Z. Sedlacek, and S.M. Mahajan, Phys. Fluids B **5**, 2999 (1993).

[51] R.D. Hazeltine and J.D. Meiss, *Plasma Confinement*, (Addison-Wesley Publishing Co. 1992).

[52] H.R. Strauss, Phys. Fluids **20**, 1354 (1977).

[53] J.D. Meiss and R.D. Hazeltine, Phys. Fluids B **2**, 2563 (1990).

[54] R. Dewar and Y.Z. Zhang, Bull. Am. Phys. Soc. (1992).

[55] S.M. Mahajan, Phys. Fluids **27**, 2238 (1984).

[56] A. Hasegawa and L. Chen, Phys. Fluids **19**, 1924 (1976).

VITA

Xiao-Dong Zhang was born on October 27, 1964, in Xinyu, Jiangxi, The People's Republic of China, the son of Tingfu Zhang and Huaying Zhang. Upon graduating from high school, he entered Tsinghua University in Beijing, China, and received the degree of Bachelor of Science in electrical engineering in July 1986. The following fall he entered The University of Texas at Austin as a graduate student in physics. He has been employed as a research assistant in the Institute for Fusion Studies since 1989.

Permanent address: Changqing school
Xinyu, Jiangxi
The People's Republic of
China

This dissertation was typeset[1] with LaTeX by the author.

[1] LaTeX document preparation system was developed by Leslie Lamport as a special version of Donald Knuth's TeX program for computer typesetting. TeX is a trademark of the American Mathematical Society. The LaTeX macro package for The University of Texas at Austin dissertation format was written by Khe-Sing The.